TURUN
YLIOPISTO
UNIVERSITY
OF TURKU

THE NATURE AND RATES OF FAILED, RARE, OR OBSCURED CORE-COLLAPSE SUPERNOVAE AND NUCLEAR TRANSIENTS

Thomas Michael Reynolds

TURUN YLIOPISTON JULKAISUJA – ANNALES UNIVERSITATIS TURKUENSIS
SARJA – SER. AI OSA – TOM. 653 | ASTRONOMICA – CHEMICA – PHYSICA – MATHEMATICA | TURKU 2021

TURUN
YLIOPISTO
UNIVERSITY
OF TURKU

THE NATURE AND RATES OF FAILED, RARE, OR OBSCURED CORE-COLLAPSE SUPERNOVAE AND NUCLEAR TRANSIENTS

Thomas Michael Reynolds

TURUN YLIOPISTON JULKAISUJA – ANNALES UNIVERSITATIS TURKUENSIS
SARJA – SER. AI OSA – TOM. 653 | ASTRONOMICA – CHEMICA – PHYSICA – MATHEMATICA | TURKU 2021

University of Turku

Faculty of Science
Department of Physics and Astronomy
Astronomy
Doctoral programme in Physical and Chemical Sciences

Supervised by

Prof. Seppo Mattila
Department of Physics and Astronomy
University of Turku
Turku, Finland

Assist. Prof. Morgan Fraser
School of Physics
University College Dublin
Dublin, Ireland

Doc. Erkki Kankare
Department of Physics and Astronomy
University of Turku
Turku, Finland

Reviewed by

Assoc. Prof. Douglas C. Leonard
Department of Astronomy
San Diego State University
San Diego, USA

Prof. Heikki Salo
Department of Physics
University of Oulu
Oulu, Finland

Opponent

Assoc. Prof Suvi Gezari
(1) Department of Astronomy
University of Maryland
Baltimore, USA

(2) Space Telescope Science Institute
Baltimore, USA

ISBN 978-951-29-8650-7 (PRINT)
ISBN 978-951-29-8651-4 (PDF)
ISSN 0082-7002 (PRINT)
ISSN 2343-3175 (ONLINE)
Painosalama, Turku, Finland, 2021

UNIVERSITY OF TURKU
Faculty of Science
Department of Physics and Astronomy
Astronomy
REYNOLDS, THOMAS: The nature and rates of failed, rare, or obscured core-collapse supernovae and nuclear transients
Doctoral dissertation, 190 pp.
Doctoral programme in Physical and Chemical Sciences
November 2021

ABSTRACT

In this thesis, two major types of astrophysical phenomena are discussed: core-collapse supernovae and transient events associated with supermassive black holes in the nuclei of galaxies. The physical processes and observable features associated with these events are described. Three articles included in the thesis concern core-collapse supernovae and their progenitors. The remaining two consider nuclear transients associated with accretion onto a supermassive black hole. The results have implications for a variety of fields, such as late stages of stellar evolution, core-collapse supernovae and their rates, and tidal disruption of stars by supermassive black holes.

An archival search in Hubble Space Telescope data for vanishing massive stars is presented in Paper I. These can be associated with a core-collapse that fails to produce a bright supernova. We present a candidate failed supernova and discuss the implications of the discovery for the expected rate of these events. Paper II presents a study of an exceptional core-collapse supernova, SN 2016gsd. The unusual characteristics of this object are connected to the presence of circumstellar material around the progenitor star. The implications for the mass-loss experienced by the star are considered. A search for supernovae in luminous infrared galaxies is presented in Paper III. It is shown that the method of using near-infrared adaptive optics allows for discovery of supernovae close to galactic nuclei, and the implications of the new discoveries for the supernova rate in luminous infrared galaxies are considered.

Paper IV describes a nuclear transient, AT 2017gbl, discovered in a luminous infrared galaxy. The properties of this event and the host galaxy are analysed through multi-wavelength observations. A stellar tidal disruption event is considered as the most likely explanation for the transient, and the implications of that conclusion are considered. Paper V presents an archival infrared search for similar nuclear transients in a sample of luminous infrared galaxies. New discoveries are described, the transient rate is derived, and the implications for the origin of such transients are discussed.

TURUN YLIOPISTO
Matemaattis-luonnontieteellinen tiedekunta
Fysiikan ja tähtitieteen laitos
Tähtitiede
REYNOLDS, THOMAS: The nature and rates of failed, rare, or obscured core-collapse supernovae and nuclear transients
Väitöskirja, 190 s.
Fysikaalisten ja kemiallisten tieteiden tohtoriohjelma
Marraskuu 2021

TIIVISTELMÄ

Tässä väitöskirjassa käsittellään kahden tyyppisiä tärkeitä astrofysikaalisia ilmiöitä: luhistumissupernovia sekä galaksiytimien supermassiivisiin mustiin aukkoihin liittyviä transienttikohteita. Väitöskirjassa kuvataan näihin kohteisiin liittyviä fysikaalisia prosesseja ja niiden havaittuja ominaisuuksia. Väitöskirjajulkaisuista kolme käsittelee luhistumissupernovia ja niiden edeltäjätähtiä. Kaksi muuta julkaisua keskittyy transienttikohteisiin, jotka liittyvät aineen kertymiseen supermassiiviseen mustaan aukkoon. Tulokset ovat merkityksellisiä tähtien myöhäisten kehitysvaiheiden, luhistumissupernovien ja niiden esiintymisrunsauden sekä mustan aukon painovoimakentässä hajoavien tähtien ymmärtämisen kannalta.

Ensimmäisessä julkaisussa esitetään Hubble-avaruusteleskoopin arkistodataan pohjautuva katoavien massiivisten tähtien etsintä. Nämä kohteet voivat liittyä tähden ytimen luhistumiseen, joka ei johda kirkkaaseen supernovaan. Esitämme tällaisen löydön ja käsittelemme sen merkitystä. Toinen julkaisuista kattaa erityislaatuisen luhistumissupernovan SN 2016gsd tutkimuksen. Kohteen epätavalliset ominaisuudet liittyvät sen edeltäjätähteä ympäröivään aineeseen ja tähden massan menetyksen merkitystä käsitellään tutkimuksessa. Kolmannessa julkaisuista esitetään supernovien etsintäohjelma kirkkaissa infrapunagalakseissa. Lähi-infrapuna-alueen adaptiivista optiikkaa hyödyntävän havaintomenetelmän osoitetaan mahdollistavan supernovien löytämisen läheltä näiden galaksien ytimiä. Uusien supernovalöytöjen merkitystä kirkkaissa infrapunagalakseissa käsitellään julkaisussa.

Neljäs julkaisu raportoi kirkkaan infrapunagalaksin ydinalueelta löydetyn transientin AT 2017gbl. Kohteen ja sen emogalaksin ominaisuuksia analysoidaan useiden eri aallonpituuksien havainnoista. Todennäköisimpänä selityksenä esitetään tähden hajoaminen mustan aukon vuorovesivoimien vaikutuksesta ja päätelmän seurauksia käsitellään. Viides julkaisu esittää arkistodataan pohjautuvan vastaavien kohteiden infrapunaetsinnän otoksessa kirkkaita infrapunagalakseja. Uudet löydöt, kohteiden esiintymisrunsaus ja seuraukset kohteiden alkuperän kannalta käsitellään julkaisussa.

Acknowledgements

First and foremost, I thank my primary supervisor Seppo Mattila. From the moment I arrived into what felt like the middle of nowhere in a strange country, until the final months of working online thanks to a global pandemic, I have always had his support and advice through the many challenges of these years of study. Any time I felt like I couldn't get the work done, his forward looking attitude and endless enthusiasm for science set me back on the path.

My supervisor Morgan Fraser deserves thanks for drawing me into astronomy during a fateful meeting at the IoA in Cambridge. After the hook was set with the exciting project he suggested, his support, enthusiasm and affable attitude reeled me in. My final supervisor, Erkki Kankare, deserves special thanks for completing the tough task of bashing so many of my messy manuscripts into shape.

Many thanks go to the staff at the NOT and the whole studentship gang who helped make my time on La Palma so fantastic. Thanks go to all the members of the supernova group in Turku. It's been fantastic to watch it grow so much during my studies. Special thanks to Jussi Harmanen who was a friendly face in two countries where I knew almost no-one!

Thanks to the pre-examiners Douglas Leonard and Heikki Salo for their review of this work, and to Suvi Gezari for agreeing to be my opponent. I thank the Jenny and Antti Wihuri foundation; the Vilho, Yrjö and Kalle Väisälä Foundation of the Finnish academy of Science and Letters; the University of Turku foundation and the Doctoral Programme in Physical and Chemical Sciences for their financial support during my studies.

Of the too-many-to-name who contributed to my projects, I thank in particular Erik Kool, Andreas Efstathiou, Stuart Ryder, Miguel Perez-Torres, Peter Lundqvist, Luc Dessart, Mattias Ergon and Max Stritzinger.

Finally, many thanks to my parents, who invested so much of their time and energy into making sure I had every opportunity to succeed. Thanks most of all to Marlene, who I love, and who makes me happy.

October 15th 2021
Thomas Michael Reynolds

Table of Contents

Acknowledgements **5**

Table of Contents **6**

Abbreviations **8**

List of Original Publications **9**

1 Introduction **11**

2 Core-collapse supernovae **14**
2.1 Overview of stellar evolution 14
2.2 Core-collapse theory 17
2.2.1 Fe core-collapse 17
2.2.2 Failed supernovae 20
2.3 Observational properties of core-collapse supernovae 24
2.3.1 Hydrogen−rich core-collapse supernovae 25
2.3.2 Circumstellar interaction in core-collapse supernovae 33
2.3.3 Supernovae in luminous infrared galaxies 40

3 Transients related to supermassive black holes **45**
3.1 Active galactic nuclei 46
3.2 Tidal disruption events 49
3.3 Nuclear transients in luminous infrared galaxies 56
3.3.1 Arp 299−B AT1 56
3.3.2 IRAS F01004−2237 57
3.3.3 Tidal disruption event rates in LIRGs 59

4 Summary of the articles **60**
4.1 Paper I 60
4.2 Paper II 61
4.3 Paper III 62
4.4 Paper IV 63

4.5 Paper V 64

5 Future Work 66

List of References 68

Original Publications 77

Abbreviations

AO	Adaptive optics
AGN	Active galactic nuclei
AGB	Asymptotic giant branch
BB	Blackbody
BH	Black hole
BLR	Broad line region
CLAGN	Changing-look AGN
CSM	Circumstellar material
CDS	Cool dense shell
CCSNe	Core-collapse supernovae
EM	Electromagnetic
HR	Hertzsprung-Russell
HST	Hubble Space Telescope
IR	Infrared
IRAS	Infrared Astronomical Satellite
IMF	Initial mass function
LGSAO	Laser guide star adaptive optics
LIGO	Laser Interferometer Gravitational-wave Observatory
LC	Light curve
LoS	Line of sight
LBV	Luminous blue variable
LIRG	Luminous infrared galaxy
MIR	Mid-infrared
NLR	Narrow line region
NIR	Near-infrared
NS	Neutron star
PNS	Proto-neutron star
RSG	Red supergiant
RLOF	Roche lobe overflow
SED	Spectral energy distribution
SFR	Star formation rate
SMBH	Supermassive black hole
TDE	Tidal disruption event
TOV	Tolman–Oppenheimer–Volkoff
UV	Ultraviolet
WD	White dwarf
WISE	Wide-field Infrared Survey Explorer
ZAMS	Zero-age main sequence

List of Original Publications

This dissertation is based on the following original publications, which are referred to in the text by their Roman numerals:

I *T. M. Reynolds*, M. Fraser, G. Gilmore
Gone without a bang: an archival HST survey for disappearing massive stars
2015, MNRAS, 453, 2885

II *T. M. Reynolds*, M. Fraser, S. Mattila, M. Ergon, L. Dessart, P. Lundqvist, Subo Dong, N. Elias-Rosa, L. Galbany, C. P. Gutiérrez, T. Kangas, E. Kankare, R. Kotak, H. Kuncarayakti, A. Pastorello, O. Rodríguez, S. J. Smartt, M. Stritzinger, L. Tomasella, Ping Chen, J. Harmanen, G. Hosseinzadeh, D. A. Howell, C. Inserra, M. Nicholl, M. Nielsen, K. Smith, A. Somero, R. Tronsgaard, D. R. Young
SN 2016gsd: an unusually luminous and linear Type II supernova with high velocities
2020, MNRAS, 493, 1761

III E. C. Kool, S. Ryder, E. Kankare, S. Mattila, *T. M. Reynolds*, M. R. McDermid, M. A. Pérez-Torres, R. Herrero-Illana, M. Schirmer, A. Efstathiou, E. F. Bauer, J. Kotilainen, P. Väisänen, C. Baldwin, C. Romero-Cañizales, A. Alberdi
First results from GeMS/GSAOI for project SUNBIRD: Supernovae UNmasked By Infra-Red Detection
2018, MNRAS, 473, 5641

IV E. C. Kool, *T. M. Reynolds*, S. Mattila, E. Kankare, M. A. Pérez-Torres, A. Efstathiou, S. Ryder, C. Romero-Cañizales, W. Lu, T. Heikkilä, G. E. Anderson, M. Berton, J. Bright, G. Cannizzaro, D. Eappachen, M. Fraser, M. Gromadzki, P. G. Jonker, H. Kuncarayakti, P. Lundqvist, K. Maeda, R. M. McDermid, A. M. Medling, S. Moran, A. Reguitti, M. Shahbandeh, S. Tsygankov, V. U, T. Wevers
AT 2017gbl: a dust obscured TDE candidate in a luminous infrared galaxy
2020, MNRAS, 498, 2167

V *T. M. Reynolds*, S. Mattila, E. Kankare, A. Efstathiou, E. Kool, S. Ryder, M. A. Pérez-Torres
Energetic nuclear transients in luminous and ultraluminous infrared galaxies
2021, to be submitted

1 Introduction

As long as humanity has observed the night sky, it has observed that it changes. The early civilisations that recorded the movements within the heavens and noted their regularity and periodicity also remarked upon irregular events. For example, Chinese astronomers took great note of transient stars that appeared outside of the normal pattern, and then disappeared again. These "guest stars" consisted of a number of physical phenomena, such as comets and stellar eruptions, but one in particular, observed in the year 185 CE, is frequently considered to be the first observed supernova (SN): the terminal explosion of a star[1]. More supernovae (SNe) would be observed throughout the next millennia, by astronomers around the world. Some examples are SN 1006, which was bright enough that it is believed one could read by its light during the night and Tycho's SN 1572, which helped fuel the "scientific revolution" by showing that the cosmos was not unchanging. The title of Tycho Brahe's work on this object *De nova stella*, led to these "new stars" being called novae.

It was not until 1934 when SNe would receive their name at the hands of Walter Baade and Fritz Zwicky, who noted that there was a group of novae with brightness significantly larger than the rest of the nova population. In their publications on SNe, (Baade & Zwicky, 1934a,b), Zwicky and Baade presciently suggested that these luminous outbursts they had observed and called SNe represented the contraction of a star into a dense object primarily composed of neutrons, what we would now term a neutron star (NS). In broad terms, they are still correct. However, understanding the exact processes involved, and the particular fates of different massive stars has proved complex both from the theoretical and observational direction.

After making these bold claims about SNe, Zwicky embarked on an observing campaign in order to find and study these objects, discovering 120 himself over half a century. Today these efforts continue, as many transient surveys observe the entire sky every few days, discovering transients in vast numbers. As an example, the Transient Name Server[2], a widely used service for reporting transient discoveries, shows 21627 transient discoveries occurring in the year 2020, of which 2091 are classified as SNe. Our modern survey telescopes allow this huge quantity of discoveries, and other modern facilities allow detailed observation of these transients across the

[1] Some authors prefer a comet explanation

[2] `https://www.wis-tns.org`

electromagnetic (EM) spectrum as they evolve.

We now understand SNe as either white dwarf (WD) stars undergoing a thermonuclear explosion, or normal stars of sufficient mass reaching the end of their lives and triggering an explosion after their core-collapse. The study of these transients in order to understand their nature and physics has led to leaps forward in our understanding of the universe. Their intrinsic brightness means they can be observed at cosmological distances and the discovery that the thermonuclear SNe can be standardised in brightness to be used as distance indicators led to the discovery of the accelerating expansion of the universe, work that was awarded the Nobel Prize in physics in the year 2011. Studying SNe arising from massive stars gives a crucial window into the evolution of these stars in the final years of their lives, which is not well understood. The state of the star and its surroundings in these late stages can be inferred from observations of the explosion and then used in order to constrain models of stellar evolution. The rate of these events can be directly connected to the rate of star formation in their locations, an area of interest in understanding galaxy evolution.

As can be seen from the numbers for transient detections quoted above, there are far more transients than just SNe discovered in our modern surveys. A number of these transients are discovered in the nuclei of galaxies and are therefore typically associated with the supermassive black hole (SMBH) that lurks there. Black holes (BHs), singularities of theoretically infinite mass shrouded in an event horizon from which not even light can escape, have long been objects of fascination, for scientists and the public alike. Recent years have offered fantastic discoveries and successes in their study. The detection of gravitational waves from merging pairs of BHs with the Laser Interferometer Gravitational-Wave Observatory (LIGO) in 2015 has been a vindication of the theory of general relativity, and has led to the discovery of a whole new population of BHs. The image of the BH in the galaxy M87 released in 2019, created through radio observations with the Event Horizon Telescope, was another such achievement. Observing the energy released as matter falls onto a SMBH is another method of studying BHs, and the historical observation of this is what led to the understanding of the existence of SMBHs at the centre of galaxies. Through studying the transient activity associated with this accretion, we can study the environment at small scales near the BH in distant galaxies, that we would be unable to resolve in direct observations.

This thesis covers a wide range of transient phenomena, ranging from core-collapse SNe (CCSNe) and their massive progenitor stars to luminous transients occurring in the nucleus of galaxies which are driven by accretion onto the SMBH within. It focuses on ascertaining the nature of these transients and, frequently, considering the rate at which they occur. Therefore, this thesis introduction aims to provide a background in the variety of topics presented in the papers, focusing on physical processes and the observations that we can use to analyse them. In Chapter

2, CCSNe are discussed, with a brief summary of stellar evolution followed by discussion of the process of core-collapse, the failed SN phenomenon and observations of SNe arising from H-rich stars. Chapter 3 describes transients associated with accretion onto SMBHs, discussing the phenomena known as active galactic nuclei (AGN) and tidal disruption events (TDEs). Chapter 4 presents a summary of the articles included in the thesis. Finally, Chapter 5 describes future plans and opportunities for ongoing research in these fields.

2 Core-collapse supernovae

2.1 Overview of stellar evolution

CCSNe are the terminal explosions of stars, so before discussing them I give a brief and descriptive account of the birth and life of stars. Presented in Fig. 1 is a Hertzsprung-Russell (HR) diagram, which shows the absolute magnitude[1] and colour of stars observed by the recent Gaia survey. On the diagram can be seen the major stages in the life of stars, and the below will refer to the locations on the diagram and describe the physical processes occurring during this stages. Further details and the underlying physics are described in e.g. Kippenhahn et al. (2012).

Stars form when clouds of gas collapse due to gravitational attraction, and parts of this gas become dense enough to begin nuclear fusion processes. Once the clump of gas is hot and dense enough to undergo hydrogen burning, it settles and enters what is know as the "main sequence", a long period of relative stability during which the star will produce the vast majority of its luminosity from the nuclear burning of H into He. The main sequence can be seen as a prominent feature of the HR diagram shown in Fig. 1. A stars position on the main sequence depends on the mass of the star when it enters the main sequence, a value known as the zero-age main sequence (ZAMS) mass. A star with a larger ZAMS mass will be both hotter and more luminous during its time on the main sequence, placing it further leftwards and upwards in Fig. 1. While on the main sequence, a star builds up a core of He, which is not at a high enough temperature to undergo further fusion into C and O, surrounded by a shell of H. At the point that central H burning ends, due to running out of supply, a shell of burning H around the He core powers the star. The inert He core contracts as it gains mass while not producing energy, and thus heats up. This increases the rate of H shell burning, and the star becomes more luminous. This additional luminosity causes the star to expand, and therefore cool, leaving the main sequence to become a giant star, situated on the giant branch shown in Fig. 1. How long a star remains on the main sequence before this happens also depends on the ZAMS mass, as stars with a large ZAMS mass burn through their nuclear fuel more

[1] Magnitude is a common measurement of brightness used in astronomy, defined by $m_1 - m_2 = -2.5\log_{10}(f_1/f_2)$ where m_1 and m_2 are the magnitudes and f_1 and f_2 are the fluxes of two observed sources. Typically these fluxes are measured in a particular section, or "band", of the EM spectrum. A choice of a particular flux for which the magnitude is zero defines the particular magnitude system.

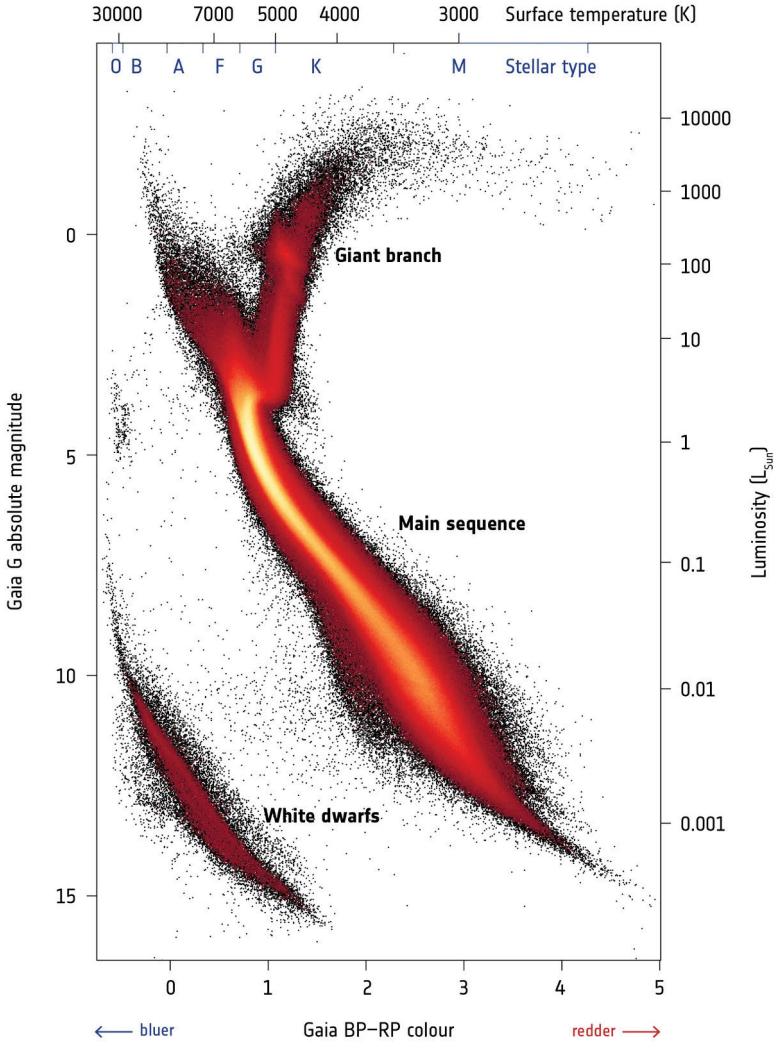

Figure 1. An example of a HR diagram, created from observations of more than 4 million stars taken from the second data release of the European Space Agency Gaia satellite. The diagram shows the major stages in the lifespan of stars and indicates how the observed colour and absolute magnitude of stars correspond to their surface temperature, luminosity ($L_\odot$ = solar luminosity), and the various spectral types that astronomers have defined.
Image credit: Gaia DPAC; Carine Babusiaux, IPAG – Université Grenoble Alpes, GEPI – Observatoire de Paris, France, CC BY-SA 3.0 IGO.

rapidly and therefore leave the main sequence earlier.

After leaving the main sequence, the He core of a star continues to increase in mass, contracting, and eventually the temperature in the centre rises to the point that He burning can begin. The star begins to form a core of C and O, as a He burning shell moves outwards from the core. In this phase of the stars life, known as the asymptotic giant branch (AGB) phase, the star again swells to have a large radius, for similar reasons as described above for the H-shell burning giant branch phase. This causes more of its material to escape due to stellar winds, a process referred to as mass-loss. When the He shell stops burning, fresh He from ongoing H fusion can reignite it, causing pulsations in the star. All of this leads to large quantities of the stars envelope being ejected.

For a star less massive than 8 $M_{\odot}$, where $M_{\odot}$ is defined as the solar mass, central temperatures will not become high enough to burn the central C and O core. Eventually burning ceases, and the CO-core is left behind, enshrouded by the stellar envelope that was previously ejected. The CO$-$core contracts until electron degeneracy pressure, produced as a consequence of the Pauli exclusion principle, can support it, ceasing the contraction and leaving the core as a slowly cooling WD (see the bottom left of Fig. 1). If a star has a ZAMS mass less than approximately 0.5 $M_{\odot}$, then He burning will never start, the AGB phase never takes place, and a He WD is left as the remnant.

Stars more massive than 8 $M_{\odot}$ are known as "massive stars". These stars are rare, making up less than 1% of the total number of stars formed (Kroupa, 2002). Massive stars will first undergo similar processes as described above, burning He into C and O and expanding to become red supergiant stars (RSGs), named such as they are 10$-$1000 times more luminous than the giant stars. Some RSGs can exhibit "blue loops" in which they evolve bluewards to blue supergiants as their temperature increases due to the effect of mass loss produced by strong stellar winds, before becoming RSGs again (see e.g. Ekström et al., 2012; Salasnich et al., 1999; Meynet et al., 2015). This evolution is sensitive to the rotation, core mass and level of mass loss from the star.

It is estimated that at least 50%, and as many as 70% of massive stars exist in binary systems, in which two stars are gravitationally bound in an orbit, and the majority of these will interact through an exchange of material in their lifetime (Sana et al., 2012). This can have drastic effects on the evolution of the star (see e.g. Podsiadlowski et al., 1992; Wellstein & Langer, 1999; de Mink et al., 2013; Zapartas et al., 2019) which are beyond the scope of this overview to describe. Binarity will be discussed further in Sect. 2.3.2.

Eventually the CO core of massive stars will contract and attain high enough central temperatures to ignite and continue the nuclear burning chain to Ne and Mg, Si and then Fe. Eventually, the star will build up a core of Fe-group elements (Fe, Ni and Co). These elements have a larger binding energy per nucleon than heavier

elements, and so further fusion will not produce more energy. This sets the stage for the stars eventual core-collapse. The timescales for these later burning stages are very short compared to the stellar lifetime of ∼3-50 Myr: a few thousand years for C burning and only a few years for the heavier elements in a 10 $M_{\odot}$ star (see e.g. Limongi & Chieffi, 2006). More massive stars will pass through these stages even more rapidly. The timescales for burning the heaviest elements are shorter than the thermal timescale of the star, and so it is expected that the core burning changes are not reflected in its surface properties. However, there is evidence from observations that this is not the case - see discussion on late-times outbursts in Sect. 2.3.2.

2.2 Core-collapse theory

2.2.1 Fe core-collapse

Most massive stars will undergo an Fe core-collapse, and here I describe this process. The description will be an overview, for a much more detailed treatment and discussion of this complicated topic, see e.g. Janka et al. (2007); Janka (2012).

The Fe-core formed in the centre of a massive star is no longer producing energy through fusion, and so it contracts until supported primarily by electron-degeneracy pressure, similarly to the case of a WD. As Fe continues to accumulate, the core will reach the Chandrasekhar mass of approximately 1.44 $M_{\odot}$ (depending on composition) where election-degeneracy pressure can no longer support it, and it will begin to collapse. Just before the collapse, the core has a radius of ∼3000 km, a central temperature of $\sim 10^{10}$ K, and density of several 10^{9} g cm^{-3} (Janka, 2012). After the collapse begins, it is accelerated by processes that remove electrons and energetic photons, robbing the core of pressure. As the temperature increases to a few MeV, photons can disintegrate Fe-nuclei into $\alpha-$particles and neutrons in an endothermic reaction:

$$\gamma + \ {}^{56}_{26}\mathrm{Fe} \Longrightarrow 13\ {}^{4}_{2}\mathrm{He} + 4n \tag{1}$$

The $\alpha-$particles can then be disintegrated into protons and neutrons if the temperature rises further. The electrons in the core will be captured by the available protons and heavy nuclei:

$$e^{-} + p \Longrightarrow n + \nu \quad ; \quad e^{-} + \ {}^{56}_{26}\mathrm{Fe} \Longrightarrow \ {}^{56}_{25}\mathrm{Mn} + \nu \tag{2}$$

This neutronisation and the corresponding loss of electrons reduces the electron degeneracy pressure, allowing further collapse. The ν's produced can escape, along with their energy, until densities reach ∼10^{12} g cm^{-3}, but even at these densities the core will continue to collapse. The stars collapse will only halt when nuclear matter densities are reached, at ∼2.7x10^{14} g cm^{-3}. Once the inner core region reaches nuclear matter density, it is supported by neutron degeneracy pressure and is suddenly much less compressible. This dense and neutron rich material in the core forms a

proto−neutron star (PNS). The remaining core is still infalling and rebounds from the PNS, colliding with the other infalling material and producing a shock front (see the top left panel of Fig. 2).

It was historically predicted that the shock would then propagate out through the star and eject the stellar material, to produce the SN that we observe (Colgate & Johnson, 1960). However, this model, known as the "prompt shock model" has proven to not be correct, as the shock instead stalls at a radius of a few hundred km (see the top right panel of Fig. 2). This is due to the shock front losing much of its energy to disassociation of Fe nuclei into free nucleons in the outer core, at the cost of $\sim$9 MeV per nucleon, and to copious ν emission (Bethe, 1990). Despite much work (see Janka et al. (2007) refs 8-25), the prompt shock model has proven to not produce SNe.

However, an additional energy source is available in order to restart the shock: the $\sim 10^{53}$ erg binding energy of the PNS forming inside the shock is more than sufficient to account for the $\sim 10^{51}$ erg explosion. The PNS produces neutrinos and anti-neutrinos of all three flavours as it cools, and these neutrinos deposit energy in a layer behind the shock, which is heated and expands, producing a "hot bubble". This heating can restart the shock, and produce a successful SN explosion (see the bottom two panels of Fig. 2). However it must compete against the ram pressure produced by mass accretion onto the PNS, and there is a critical neutrino luminosity which is a function of the mass accretion rate, that will cause a successful explosion. This mechanism is known as the "delayed neutrino-driven explosion mechanism". Although this mechanism has only limited success in exploding stars in one-dimensional (1D) simulations, succeeding only in some low-mass cases, advancements in computer power and the developments of more efficient codes have led to successful explosions in two dimensions (see e.g. Janka, 2012). These successes depend on effects such as the standing accretion-shock instability (see e.g. Blondin et al., 2003; Hanke et al., 2012), that are present in the higher dimensions but not in 1D. The most recent research is beginning to move to three dimensional simulations, which is necessary to fully understand the core-collapse phenomenon (see e.g. Janka et al., 2016).

Given the energies listed above, less than a percent of the radiated neutrino energy is deposited this way in a successfully exploded star. The amount of energy that can be deposited is set by the binding energy of the shell of progenitor material close to the PNS. Once the shock is restarted and the material is unbound, it expands away from the neutrino−heating region, halting further energy deposition. This additionally provides an upper limit for the energy of the explosion of about 2.5×10^{51} erg (Janka et al., 2016).

The PNS at the core of the star accretes material until the shock is restarted and the SN successfully exploded, at which point its mass decides its fate. If it is less massive than the Tolman–Oppenheimer–Volkoff (TOV) limit of $\sim 2-3\ M_{\odot}$, then it

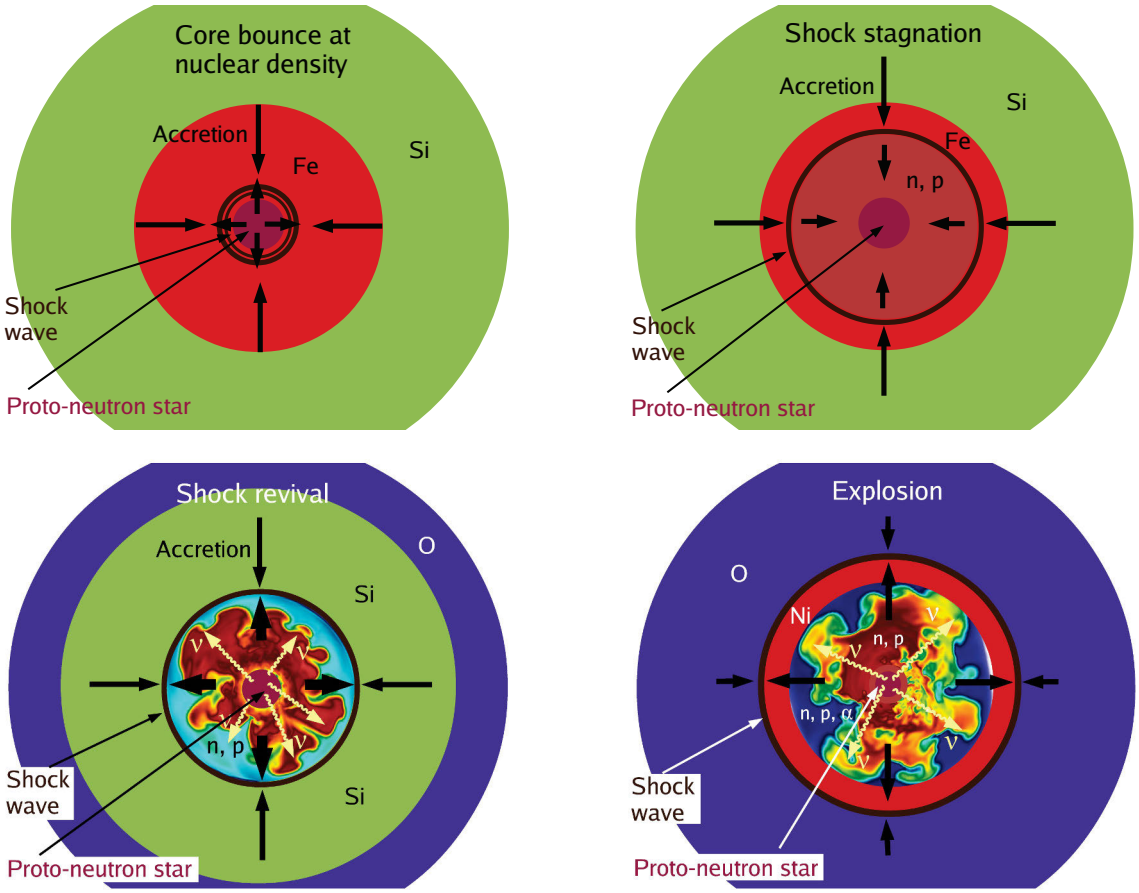

Figure 2. Schematic depiction of the inner regions of a massive star passing through the stages of evolution occurring during a core-collapse, taken from Janka (2012). Panels should be read from left to right, top to bottom. The initial core bounce and shock stagnation occurring within the Fe core are shown in the top row. The revival of the shock and following explosion are depicted in the bottom row. Note the changes of scale between panels, with the colour indicating the layers of elements within the star. The stages are described in more detail in the main text.

will continue to neutronise, as electrons are captured onto protons, becoming a NS after $\sim$10 seconds (Burrows & Lattimer, 1986), supported by neutron degeneracy pressure and the strong nuclear force. If it is more massive than this limit, it will continue to collapse into a BH, where its matter (theoretically) will reside at a singularity, a point of infinite density, inside an event horizon from which not even light can escape. The exact value of the TOV limit is not known, but recent observations of a NS merger have suggested it is $<$2.3 $M_{\odot}$ (Shibata et al., 2019; Margalit & Metzger, 2017; Ruiz et al., 2018).

2.2.2 Failed supernovae

Stars significantly more massive than 8 $M_{\odot}$ are more difficult to explode through the delayed neutrino-driven explosion mechanism. It has been suggested by numerous authors (e.g. Woosley, 1993; Fryer, 1999; O'Connor & Ott, 2011; Sukhbold et al., 2016) that in cases where the ram pressure from ongoing accretion is too high, the shock might not restart, leading to direct collapse to a BH, and a "Failed Supernova". A SN will fail if the shock does not restart before the PNS is pushed over the TOV limit and becomes a BH, as this will halt the neutrino flux.

As well as the theoretical evidence that SNe can fail, there is also observational support from the study of SN progenitors. In such study, high quality data of sites of nearby SN explosions, taken *before* they exploded, is studied in order to identify the nature of the specific star that exploded, a.k.a the progenitor. Smartt et al. (2009) and Smartt (2015) considered the sample of SN progenitor detections in the literature and inferred that there was a deficit of high mass progenitor detections, in contrast with the predicted distribution of ZAMS masses from stellar evolution theory. They calculated that the most likely maximum mass for a SN progenitor inferred from these observations was approximately 18 $M_{\odot}$. The progenitor detections are almost all RSG stars, associated with H-rich SNe (see discussion of SN types in Sect. 2.3). Other SNe are expected from theory to have higher mass progenitors, but there are very few detections of these and identifications of the progenitor systems are often uncertain and/or controversial (see e.g. Smith et al., 2011b; Cao et al., 2013; Folatelli et al., 2016; Van Dyk et al., 2018; Xiang et al., 2019; Kilpatrick et al., 2021).

Additional evidence for the lack of high mass progenitors comes from modelling of late-time spectra of SNe, where the strength of certain emission lines, particularly [O I], are dependent on the progenitor ZAMS mass. Modelling of observed SNe has yielded measurements of the ZAMS mass consistent with progenitor studies, and also lacking high mass progenitors (Jerkstrand et al., 2014), although there is at least one example of a high mass progenitor inferred from late time spectroscopy (Anderson et al., 2018). One solution for this dearth of high mass progenitors would be if these stars are directly collapsing to BHs.

It should be noted that some authors doubt that the progenitor observations sup-

port a lack of high mass progenitors. The conversion of single band progenitor flux measurements to bolometric luminosities and estimates of extinction produced by material around the progenitor introduce large uncertainties in the final measured progenitor mass, and corrections performed by Davies & Beasor (2018) re-evaluate the maximum statistical progenitor mass estimate as 33 $M_{\odot}$, at 2σ significance. Additionally, the sample of SN progenitors we observe is biased towards stars with low extinction, and host galaxies with high metallicity, as these are the progenitors for which archival detections are available, which could yield an unrepresentative progenitor sample (Davies & Beasor, 2020).

Exactly which stars will collapse directly to a BH, and what exactly the remnant and any luminous outburst will look like, are matters of active research. Fryer (1999) suggested from their modelling that stars more massive that $\sim$25 $M_{\odot}$ would form a BH, while stars more massive than $\sim$40 $M_{\odot}$ would directly collapse. O'Connor & Ott (2011) made use of a 1.5D general relativistic code to model the collapse process, and find the key parameter determining the stars fate to be the "compactness parameter":

$$\xi_M = \left. \frac{M/M_{\odot}}{R(M_{\rm bary} = M_{\odot})/1000{\rm km}} \right|_{t=t_{\rm bounce}}. \tag{3}$$

Here, $R(M_{\rm bary} = 2.5M_{\odot})$ is the radial coordinate that encloses 2.5 $M_{\odot}$ at the time of core bounce, and $\xi_{2.5}$ measures the compactness of the core at bounce, with 2.5 $M_{\odot}$ chosen as the relevant mass scale for BH formation. The importance of this parameter is that, following a simple application of Kepler's third law to a free falling mass element (see section 4.4 of O'Connor & Ott (2011)), the time available for the shock to restart follows $t \propto \xi_{2.5}^{-3/2}$.

The interesting result of this is that there is not a simple cut in ZAMS mass above which BHs form, or SNe fail, but a non-monotonic relationship, where "islands of explodability" exist in the ZAMS mass function for stars whose evolution lead to less compact cores. Sukhbold et al. (2016) analysed the explodability of stars across the entire ZAMS mass range and found that the results varied extremely non-monotonically (see Figure 3), with stars reliably exploding up to a ZAMS mass of $\sim$15 $M_{\odot}$ followed by a region of "islands of explodability", where certain mass ranges exploded and others failed (see also Ertl et al., 2016). These results become more uncertain for stars more massive than $\sim$30 $M_{\odot}$, where stellar mass loss becomes very significant (see Sect. 2.3.2).

For very high ZAMS mass stars, greater than $\sim$100 $M_{\odot}$, it is possible that they do not undergo core-collapse and instead end their lives with pulsational pair-instability or pair-instability SNe, in which the production of electron-positron pairs in the extremely hot ($>10^9$ K) stellar core causes a drop in radiation pressure that can disrupt and destroy the star (see e.g. Heger & Woosley, 2002; Woosley et al., 2007). However, it is expected that only a star with low enough metallicity to avoid extreme mass

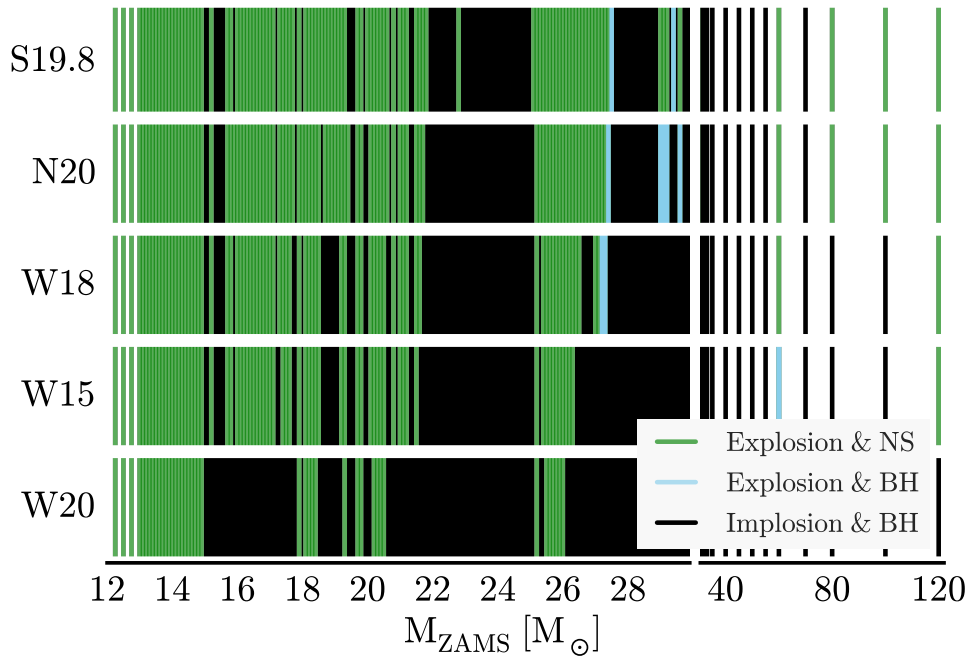

Figure 3. This figure taken from Sukhbold et al. (2016) shows the fate of stars with various ZAMS mass. The modelling is calibrated to observations of SN 1987A and its progenitor, with each row representing different progenitor and PNS properties for this calibration, taken from literature. Whether a star successfully explodes or directly collapses (implodes) is a non-monotonic function of ZAMS, with many "islands of explodability."

loss through its lifetime can undergo such an explosion.

In the case of a failed SN, there may still be some form of observable signal. During PNS formation, energy loss to neutrinos can cause a mass loss of a few tenths of a $M_{\odot}$ over a period of a few seconds. This is shorter than the sound crossing time through the outer core composed of He and heavier elements, and the neutrinos barely interact with material outside the Fe core. Thus, to the outer parts of the star, the effect is that the gravitational potential has suddenly decreased, and this causes the outer star to expand. Nadezhin (1980) made the first theoretical predictions of the results of this phenomena, and more recently Lovegrove & Woosley (2013) find that, in some cases, this expansion can unbind the hydrogen envelope of the star, but that the precise neutrino mass loss history and the structure of the CO and He core of the star has a strong effect on the shock produced by the expansion. If the H envelope is unbound, the transient produced will be long lasting, low energy, and red, with much of the emission coming from the H recombination of the ejected envelope. Piro (2013) explored the shock breakout signature from such an event with the same models, and predicted a short (3-10 day), blue (T$\sim$10000 K) and low velocity ($<$ 200 km s^{-1}) transient, with a H-dominated spectrum. There are other types of transients associated with failed SNe such as the "collapsar", in which stellar material that is not ejected in the core-collapse falls back onto the PNS, promptly forming a BH and accretion disk, which could launch jets, and would be associated with relatively long-lived (a few tens of seconds) gamma ray signals (MacFadyen et al., 2001; Woosley & Heger, 2012).

Finding observational constraints on the rates of failed SNe, or direct observations of the transients associated with them described above, would bring us closer to understanding the lack of high mass SN progenitors, constrain the transients associated with failed SNe and characterise the formation channels and initial masses of BHs. In order to do this, Kochanek et al. (2008) suggested what they described as "A Survey about Nothing": repeated observational monitoring of nearby galaxies in order to detect individual vanishing massive stars corresponding to failed SNe. This would also be likely to observe, or set limits on, any transients associated with this vanishing, depending on the survey cadence. With or without a detection, they could set rates for failed SNe within a volume limited sample.

Such a search has been carried out, and is described in Gerke et al. (2015); Adams et al. (2017a,b); Neustadt et al. (2021). The authors monitored 27 nearby galaxies over 11 years in order to identify vanishing stars, and found and confirmed one strong candidate, known as N6946-BH1. The target was identified as an object that underwent an outburst before diminishing by 5 magnitudes. Pre-explosion Hubble Space Telescope (HST) images were consistent with a 25 $M_{\odot}$ RSG, placing the candidate in a region where the compactness parameter is high (O'Connor & Ott, 2011; Sukhbold et al., 2016), making the star a good candidate for a failed SNe. The outburst was broadly consistent with that predicted by Lovegrove & Woosley (2013)

but poorly constrained by observation. However, at late times the object returned to pre-explosion luminosity at mid-infrared (MIR, here defined as $\sim$2.5-8μm) wavelengths. The authors note that the bolometric luminosity is less than pre-explosion, indicating the initial star has not survived, and suggest that fallback accretion onto the newly formed BH contained within a cocoon of obscuring dust created during the outburst could explain this. Ongoing observations (Basinger et al., 2020) reveal that the star remains missing, and a failed SN is the most likely explanation. Assuming that this object is a failed SNe, the fraction of massive stars that undergo failed SNe is calculated as $0.16^{+0.23}_{-0.12}$. The survey has recently obtained another candidate, that will require further observation to classify as a failed SN or rule out (see Neustadt et al., 2021). A search for failed SNe in archival HST data is described in Paper I. We report the discovery of a failed SN candidate, where a source consistent with a $25-30\ M_{\odot}$ star appears to have disappeared.

The recent and groundbreaking detection of gravitational waves from BH$-$BH mergers with the LIGO (Abramovici et al., 1992; Abbott et al., 2009) has brought new insights into the population of compact SN remnants. The multiple laser interferometers that make up this observatory detect the strain of gravitational waves created by inspiralling close binary systems of BHs or neutron stars in the last stages of merging and, through analysis of the signal produced, can infer properties of the compact objects. Some detected signals, such as GW151226 (Abbott et al., 2016), arose from the merger of BHs with somewhat low masses: $7.5^{+2.3}_{-2.3}\ M_{\odot}$ and $14.2^{+8.3}_{+3.7}$ $M_{\odot}$ in this case. These measured masses overlap with the observed population of BHs detected through X-ray observations (see e.g. Remillard & McClintock, 2006), and are consistent with their formation in a binary star system in which both stars underwent core$-$collapse, although the precise formation channels for these systems is an area of intense research (see e.g. Langer et al., 2020). The properties of the new population of BHs detected by LIGO could potentially be used to constrain the types of SN that lead to BHs (see e.g. Schrøder et al., 2018), which would have consequences for the ZAMS mass ranges that lead to failed SNe.

2.3 Observational properties of core-collapse supernovae

Although most massive stars undergo a broadly similar process of core-collapse, the condition of the star and its surroundings at the time of this event will create a great variety in the properties of the CCSNe that we observe. The first fundamental distinction, noted by Minkowski (1941), is between those SNe that have H emission features, known as Type II, and those that do not, known as Type I. SNe were further sub-divided into various subclasses, summarised by Filippenko (1997), according to other spectral and photometric features, and there have been further classes and subdivisions made since (see Gal-Yam, 2017, for recent summary). Spectra of the

various CCSNe subtypes are shown in Fig. 4.

The H-rich SNe were divided into Type IIP and Type IIL for "Plateau" and "Linear" respectively, based on the presence or lack of a $\sim$ 100 day phase of roughly constant luminosity in their evolution (Barbon et al., 1979). SNe that showed H at early times but later evolved to not have H features were titled Type IIb SNe (Filippenko et al., 1993). An additional subtype of Type II SNe was described by Schlegel (1990), who identified SNe that showed narrow H emission lines with wings characteristic of electron scattering in a dense medium as Type IIn SNe ("n" for "narrow"). The SNe without H were first divided into those with a strong Si II absorption feature, known as Type Ia, and those without, which were further sub-divided into those which show He features, called Type Ib (Wheeler & Levreault, 1985; Elias et al., 1985), and those with neither H nor He, Type Ic (Wheeler & Levreault, 1985; Filippenko et al., 1995). Some Type Ib SNe show narrow emission lines of He, similar to those seen in Type IIn SNe, leading to them being named Type Ibn (Pastorello et al., 2007). Also discovered were Type Ic-BL SNe: Type Ic SNe with broad, high velocity ejecta and broad, shallow absorption lines, which are associated with gamma ray bursts (Galama et al., 1999; Iwamoto et al., 2000; Patat et al., 2001). Type Ia SNe are the thermonuclear explosion of WD stars, rather than CCSNe, and thus I will not discuss them further in this work. In this chapter, observational features of CCSNe are discussed, focusing primarily on Type II SNe, and we explore the physics that causes these features.

2.3.1 Hydrogen−rich core-collapse supernovae

As discussed above, at the end of their lifetime a large proportion of massive stars will be RSGs. At this point, they are expected to have some amount of H left in their envelope, as well as a layered structure of heavier elements deeper within. This expectation is supported by volume limited surveys that have found 75% of CCSNe to be Type II SNe (Li et al., 2011), which show H in their spectra and have luminosity evolution greatly influenced by this material. Here I describe the explosion of a "typical" RSG with a ZAMS mass of 10-15 $M_{\odot}$, as it passes through several post core-collapse stages, characterised by their power source.

Once a shock has been successfully restarted through the delayed-onset neutrino mechanism in a star that undergoes core-collapse, it will propagate outwards through the star, unbinding it and ionising the material. The earliest observable EM radiation from the SN is the "shock breakout". While the shock front is deep inside the star, the region in front of it is optically thick and the influence of the shock can not be observed from outside the star. The size of the zone in front of the shock influenced by radiation can be estimated by comparing the timescale of radiative diffusion, $t_d = 3(\delta R)^2/cl$, where l is the photon mean free path, to the timescale of the advance of the shock front, $t_{\delta R} = \delta R/v$, where v is the shock velocity (Arnett, 1996). While

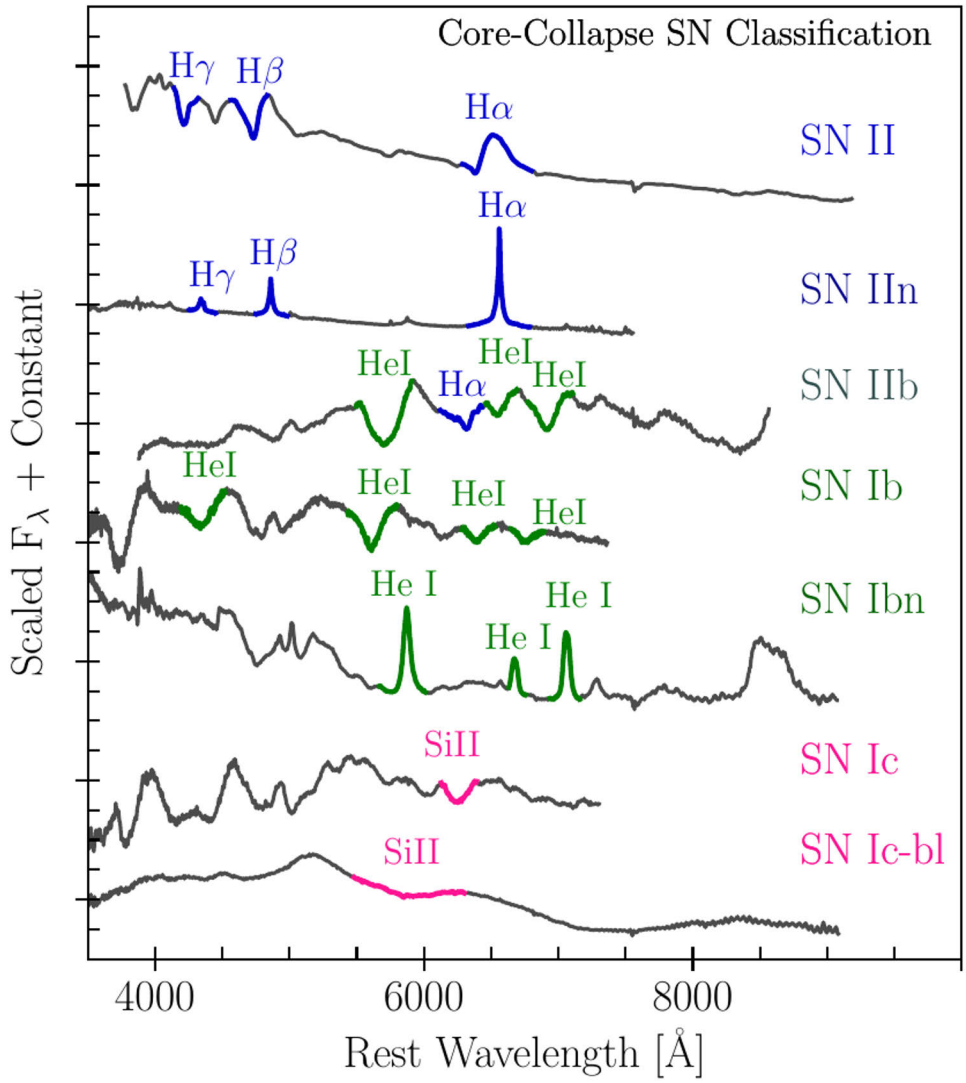

Figure 4. Figure taken from Modjaz et al. (2019) showing spectra characteristic of the major CCSN subtypes. The key features used to classify the different subtypes are highlighted.

$t_d > t_{\delta R}$, the radiation remains trapped in the stellar envelope. Once $t_d < t_{\delta R}$ the trapped photons can escape, and shock breakout occurs. Rearranging this condition we see it is equivalent to:

$$\tau = \frac{\delta R}{l} < \frac{c}{3v} \tag{4}$$

i.e. the shock breakout occurs when the optical depth, τ, between the shock front and the stellar photosphere is comparable to c/v (Ohyama, 1963).

At this point, the light that was trapped inside the shock "breaks out" with a bright flash that lasts only seconds to hours. The spectrum of the breakout emission depends on the shock front velocity. For the H-rich CCSNe discussed in this chapter, it will peak in the ultraviolet (UV), but for stars with more compact envelopes and higher energy explosions, it can peak in X-ray or gamma rays (for more detail see e.g. Levinson & Nakar, 2020). The shock breakout has been observed in both UV and optical in a few cases where there are high cadence early-time observations (e.g. Garnavich et al., 2016; Gezari et al., 2015; Schawinski et al., 2008). For a few days after the shock breakout, the outer parts of the stellar envelope, which was heated by the passage of the shock, will dominate the ongoing emission as it expands and cools (Waxman & Katz, 2017). The radiation from deeper in the envelope remains trapped, and the emission depends strongly on the progenitor radius and the expansion velocity, providing unique observational tracers of these parameters (see e.g. Gezari et al., 2010). After this short phase, these material will cool and the photosphere (the emitting surface, typically defined as where $\tau = 2/3$) recedes (in mass coordinates) into the outer shell of the envelope.

After the shock breakout and cooling phase of a few days, SNe enter their "photospheric phase". During this period, the stellar envelope is composed of an ionised plasma that is expanding homologously, so that the velocity of a fluid element is proportional to its radial position. The innermost layers of the star move more slowly as they have lost most of their kinetic energy and momentum to the outer layers (Zampieri et al., 2003). The energy deposited within the envelope is approximately split evenly between kinetic and internal energy (Kasen & Woosley, 2009) and during the evolution the internal energy will be lost both to expansion and radiation. For a few tens of days the envelope will remain optically thick to radiation, and the luminosity observed is derived by diffusion of photons. The luminosity during this period will be greater for stars with less massive envelopes, all else being equal, as the mean free path of the photons will be larger. Additionally, SNe with a more extended initial ejecta will be brighter, given fixed thermal energy and mass, as less internal energy will be spent on expansion. (This can be seen from Equation 13.17 in Arnett (1996)).

As energy is lost to radiative diffusion and expansion, the temperature of the envelope will decrease. At some temperature, depending on the chemical composition

of the envelope, the plasma will begin to recombine. For a H−rich envelope, the case we consider, this will be at ∼6000 K. The envelope will then be divided into two regions by a recombination front, now the effective photosphere, above which the envelope is mostly transparent to optical photons, and below which it is still optically thick. Below the recombination front, energy is still lost to diffusive radiation as above (with some caveats, see Arnett (1996)), with additional energy being released from recombination itself. These two energy sources are similar in magnitude (see Arnett, 1996), and will dominate the luminosity until the recombination front has swept through all the ejecta.

There is an additional major energy source for SNe throughout their evolution: that of radioactive heating. It was noted by some of the first observers of SNe (Baade, 1945) that after ∼100 days, SNe luminosity would exponentially decline, and radioactive decay was intuitively suggested as the source by Borst (1950). Colgate & McKee (1969) identified that the decay chain powering this was that of ^{56}Ni $\longrightarrow^{56}$ Co $\longrightarrow^{56}$ Fe. These decays take place via electron captures and β^+-decays, which produce gamma-ray photons and positrons, which will also annihilate to gamma rays. If the SN ejecta are optically thick to these gamma rays, which will be the case for a typical IIP SNe for approximately a few hundred days (Arnett, 1996; Zampieri et al., 2003), they will deposit their energy into the SN ejecta. This energy source is much less than that provided by recombination and radiative diffusion during the photospheric phase of a Type II SNe, so is not observable while the recombination front recedes through the ejecta. However, at late times once the recombination energy is exhausted, this energy will become dominant (assuming no input from CSM interaction, see Sect. 2.3.2) and the SNe will enter the radioactively powered "tail" phase. The decay from ^{56}Ni $\longrightarrow^{56}$ Co has an e-folding time[2], $\tau = 9$ days, so will not be significant during the tail phase, but the second reaction has an e-folding time of τ =111 days and as the photospheric phase of a typical Type II is ∼80 days (e.g. Anderson et al., 2014b), this decay powers the tail phase.

These 3 phases can be noted in the observed light curves (LCs) of Type II SNe. In Fig. 5 are shown some examples of SN observations in the V-band (approximately 4900−5900Å). Notable is that some of the Type II SNe shown (SN 1999em (Leonard et al., 2002) and SN 2004et (Maguire et al., 2010)) exhibit a period between around 30−100 days post-explosion where they have approximately constant magnitude (e.g. Anderson et al., 2014b). These SNe are named Type IIP SNe, for this "plateau" period in their LC (Barbon et al., 1979; Doggett & Branch, 1985). The plateau period corresponds to the photospheric phase described above, where the recombination front is receding through the H-rich ejecta. The approximately constant luminosity comes from a balance between the recession of the photosphere into

[2]The e-folding time τ is defined $\tau := \frac{t_{1/2}}{\ln 2}$, where $t_{1/2}$ is the isotope half-life. It characterises the decay rate of the isotope.

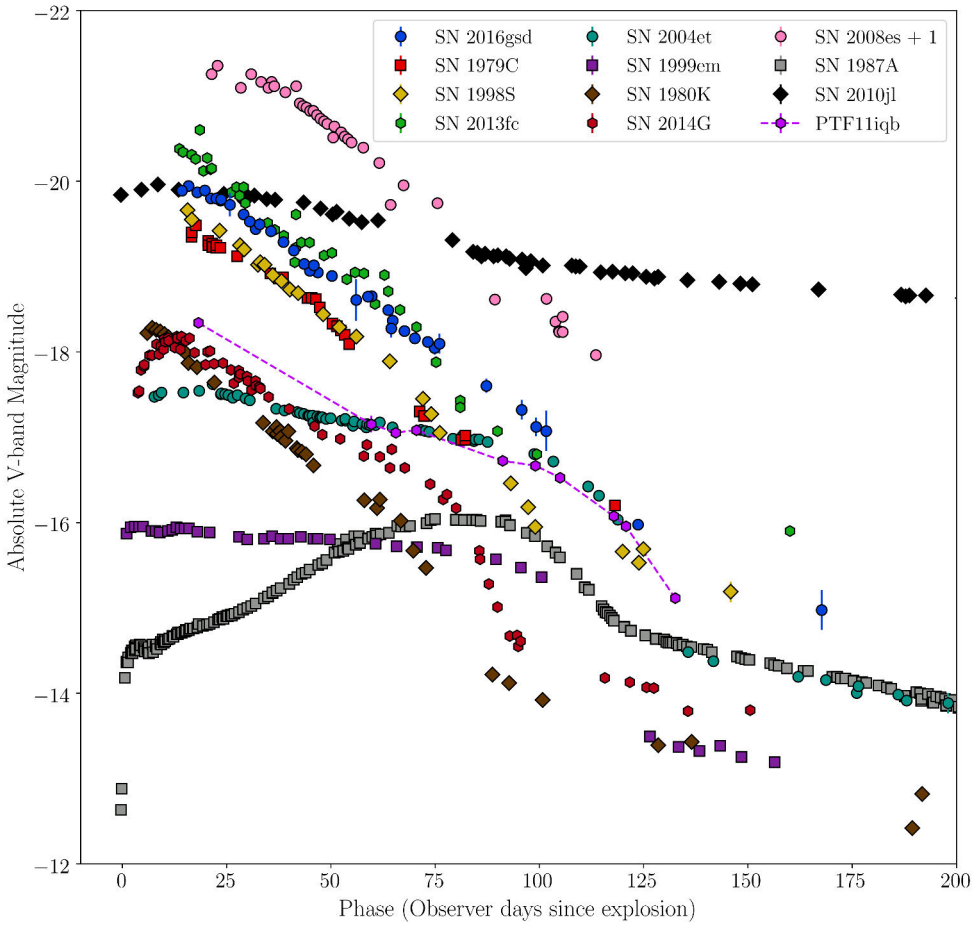

Figure 5. A comparison of Type II CCSN V-band LCs. The photospheric and tail phases of evolution described in Sect. 2.3.1 are clearly visible in many objects, but less clear in the brighter Type IIL SNe. Figure adapted from Paper II, with additional data and parameters taken from Smith et al. (2015); Fransson et al. (2014); Maguire et al. (2010) and Leonard et al. (2002).

deeper layers of the ejecta with the overall expansion of the ejecta. This keeps the radial coordinate of the photosphere approximately constant, and as described above the temperature is fixed at the recombination temperature of H, leading to a plateau in luminosity. After the end of the plateau there is a sudden drop in luminosity as the dominant energy source becomes the radioactive decay, and we begin to observe the tail phase.

The spectra of Type IIP SNe, (see SN 2004et in Fig. 6) typically show broad emission lines of H at approximately the rest wavelength, as well as blueshifted broad absorption features also associated with H. This feature is known as a "P-Cygni" profile, named after a notable variable star in which this line profile is observed (Maury & Pickering, 1897). This line profile is created in P-Cygni by an expanding stellar envelope (McCrea, 1929; Beals, 1929) and in the case of SNe, the expanding ejecta. The part of the expanding recombined H envelope that is projected against the photosphere absorbs part of the continuum emission from this photosphere, producing an absorption line. As the material in the envelope is moving towards the observer, the absorption line is blueshifted an amount corresponding to its velocity. The remainder of the envelope, instead projected against the background sky, produces a broad emission line as it recombines (see e.g. Castor & Lamers, 1979, for more discussion).

Notably, the emission line profiles of H we observe in Type II SNe are not symmetrical at early times, instead showing a blueshift of a few 1000 km s^{-1} (Anderson et al., 2014a). This is due to occultation of the emitting region on the far side of the explosion by the dense inner regions of the ejecta (Dessart & Hillier, 2005). This is a particular feature of P-Cygni profiles in SNe, as compared to those observed in stars, due to the steep density profile in the ejecta causing the emitting H to lie very close to the photosphere, and thus be more easily occulted (Anderson et al., 2014a). This effect dwindles as the recombination front recedes and more of the ejecta become optically thin, with the emission profile eventually centred at the rest wavelength.

Type IIL SNe were originally defined (Barbon et al., 1979) in contrast to Type IIP, having somewhat similar spectral features but lacking the defining plateau in their luminosity. The distinction has been supported by a number of studies (e.g. Patat et al., 1994; Arcavi et al., 2012; Faran et al., 2014), but more recent research has cast doubt on whether Type IIL SNe represent a different subclass of objects from Type IIP, or a continuous group (e.g. Anderson et al., 2014b; Sanders et al., 2015; Galbany et al., 2016; Rubin et al., 2016). This latter group of studies has larger sample sizes than previous work, and Type IIL SNe make up only 10% of Type II (Li et al., 2011), so it is to be expected that large sample sizes would be required to investigate whether they form a group that is discrete or continuous with Type IIP. Considering the LC of a typical Type IIL SNe (see SN 1980K (Barbon et al., 1982) and SN 2014G (Terreran et al., 2016) in Fig. 5), we see a similar 3-phase structure in the LC to that of Type IIP SNe, with the crucial difference being that the plateau phase in Type IIP is instead a period of decline in Type IIL SNe. It can be intuited

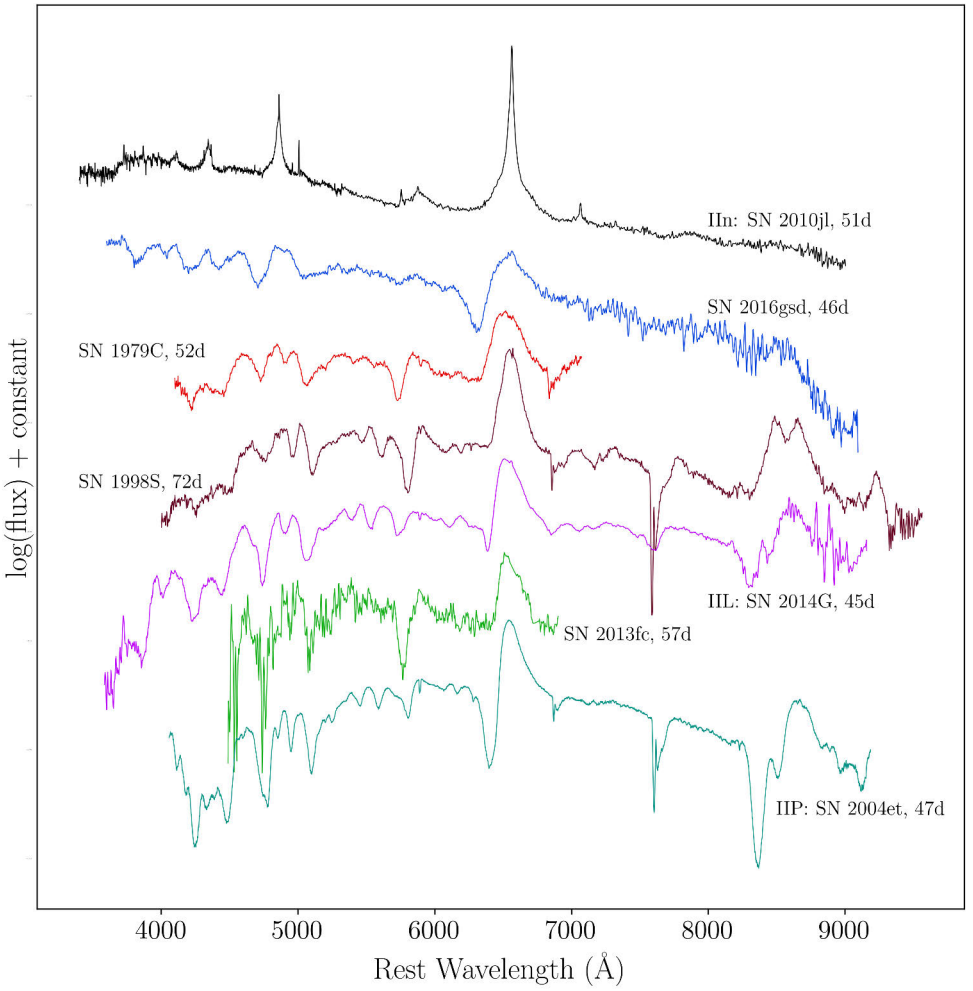

Figure 6. A selection of spectra of Type II SNe, taken approximately 50d after explosion. Somewhat typical Type IIn, IIP and IIL SNe are shown and labeled. The remaining objects are luminous SNe with linear LCs. These objects are all affected by CSM interaction to some extent, although not all are classified as Type IIn. A notable feature of the spectra is that SN 2016gsd shows a strong H absorption feature in its P Cygni profile, in contrast to the other luminous linear SNe such as SN 1979C and SN 1998S. Adapted from Paper II, with the addition of data of SN 2004et (Maguire et al., 2010) and SN 2010jl Fransson et al. (2014).

that the periods of evolution represent similar physical processes. Indeed Valenti et al. (2015) claim that all Type IIL SNe that are followed for sufficiently long will exhibit a drop from the photospheric phase to a tail phase except perhaps the SN 1979C (which will be discussed in more detail below). Furthermore, Anderson et al. (2014b) note that many IIP SNe have slow linear decline rates during the plateau, to the point where it is difficult to construct a definition of Type IIL SNe consistent with historical usage from the criterion of total decline over the $\sim$80d plateau period.

This indicates that Type IIL and Type IIP SNe could come from the same population of progenitors, and we should instead consider them as one class of Type II SNe with "linear−ness", measured as their decline rate during the photospheric phase, a continuously distributed parameter. In this framework, we can note that "more linear" SNe are systematically more luminous, exhibit faster velocities and have weaker H absorption features than less linear SNe (Faran et al., 2014; Anderson et al., 2014b; Valenti et al., 2015; Sanders et al., 2015). A suggested explanation for these observational features is a less massive H envelope. With less H-rich material, the optical depth within the envelope would be reduced and stored radiation would be released more rapidly during the photospheric phase, leading to the faster decline (Grassberg et al., 1971; Blinnikov & Bartunov, 1993). As noted above, the peak luminosity will also increase for a less massive and/or more extended envelope, consistent with this explanation. Additionally, this could explain the less strong H-absorption feature (see SN 2014G in Fig. 6) as due to a lower column density of absorbing material.

The relative rareness of Type IIL SNe leads to speculation that they could arise from higher mass progenitors than Type IIP, which are less common following the initial mass function (IMF) (Salpeter, 1955). This would be consistent with their higher velocities, a potential indicator of higher explosion energies that are linked to larger ZAMS mass stars; as well as their relatively H-poor envelope, which could be due to mass loss from line-driven winds that is stronger in more massive stars. However, due to their rareness only very few progenitor detections have been possible so far, although Maund et al. (2015) limits the ZAMS mass of the progenitor of Type IIL SN 2009kr to $<$25 $M_{\odot}$ and Elias-Rosa et al. (2011) finds $<$20 $M_{\odot}$ for the Type IIL SN 2009hd.

Although Type IIP and IIL SNe are now often considered to be a continuous class of objects, possibly representing a transition from less to more massive progenitors, with different H envelope properties, there are a number of SNe that have been or could be described as "linear" SNe, but are quite separated from this continuous group by their luminosity. Members of this group are shown in Fig 5 and are approximately 2 magnitudes brighter than the typical IIP/IIL SNe such as SN 2004et and SN 1980K. It includes SN 1979C (Branch et al., 1981), a well known Type IIL SNe that was long considered to characterise the class, and SN 1998S (Fassia et al., 2000, 2001; Leonard et al., 2000) which has a very similar luminosity evolution. The evolution of these objects is influenced by interaction between the SN ejecta and a

circumstellar material (CSM) around the progenitor star and in order to understand these objects, we must first discuss this phenomena.

2.3.2 Circumstellar interaction in core-collapse supernovae

Many CCSNe show signatures of interaction with CSM. This is to be expected, as massive stars are strongly effected by mass loss, in which parts of their envelope become gravitationally unbound through a variety of physical mechanisms throughout their lives (See e.g. Lucy & Solomon, 1970; Humphreys & Davidson, 1994, and refs below). The rapidly expanding ejecta from a CCSN will collide with the slowly moving CSM and, depending on the CSM density and distribution, convert some of the kinetic energy of the explosion into radiated energy. The total radiated energy of a "normal" Type II CCSN will typically only be $\sim$1% of their kinetic energy, Therefore, more efficient conversion of the kinetic energy into internal and radiated energy can greatly increase the total SN luminosity. Furthermore, the interaction signatures can be observed in spectroscopic features, as well as detected in X-ray and radio observations.

Schlegel (1990) defined Type IIn SNe as objects showing narrow emission lines of H superimposed on broad Lorenztian wing features in their spectra, along with a blue continuum (see SN 2010jl in Fig 6). These signatures strongly identify interaction, as the narrow core of the H emission originates from the recombination of unshocked CSM gas, excited by light from the SN, with the broad emission line wings produced by electron scattering occurring in the dense CSM (Chugai, 2001). Within CCSNe that show this feature, there is a great deal of variety in LCs, as shown in Fig. 7. The peak luminosity of these events spans a range of $>$4 magnitudes, and the rise and decline rates vary greatly. This can be attributed to the variety of densities, masses, and configurations of the CSM surrounding them, as well the nature of the underlying SN.

To describe the physical processes occurring in interacting SNe, we can consider a simple configuration of spherical CSM, shown schematically in Fig. 8. The first interaction between the SN and CSM occurs at the shock breakout, at the point the X-ray/UV light escapes the stellar surface. These energetic photons ionise the CSM and the effects can be observed in narrow emission lines from highly ionised species. This was observed in Type IIn SNe such as SN 1998S, where C III and N III emission lines were present in early spectra and quickly vanished (Fassia et al., 2001). High ionisation lines that vanish after a few days are also seen in other SNe not classified as Type IIn when they are observed spectroscopically very soon after explosion (see e.g. Gal-Yam et al., 2014; Khazov et al., 2016; Tartaglia et al., 2021), indicating the presence of CSM. As discussed in Sect. 2.3.1 the shock breakout occurs when the optical depth in front of the shock is sufficiently low. Thus, if the CSM is dense enough, the shock breakout can occur while the shock is in the CSM, rather than in

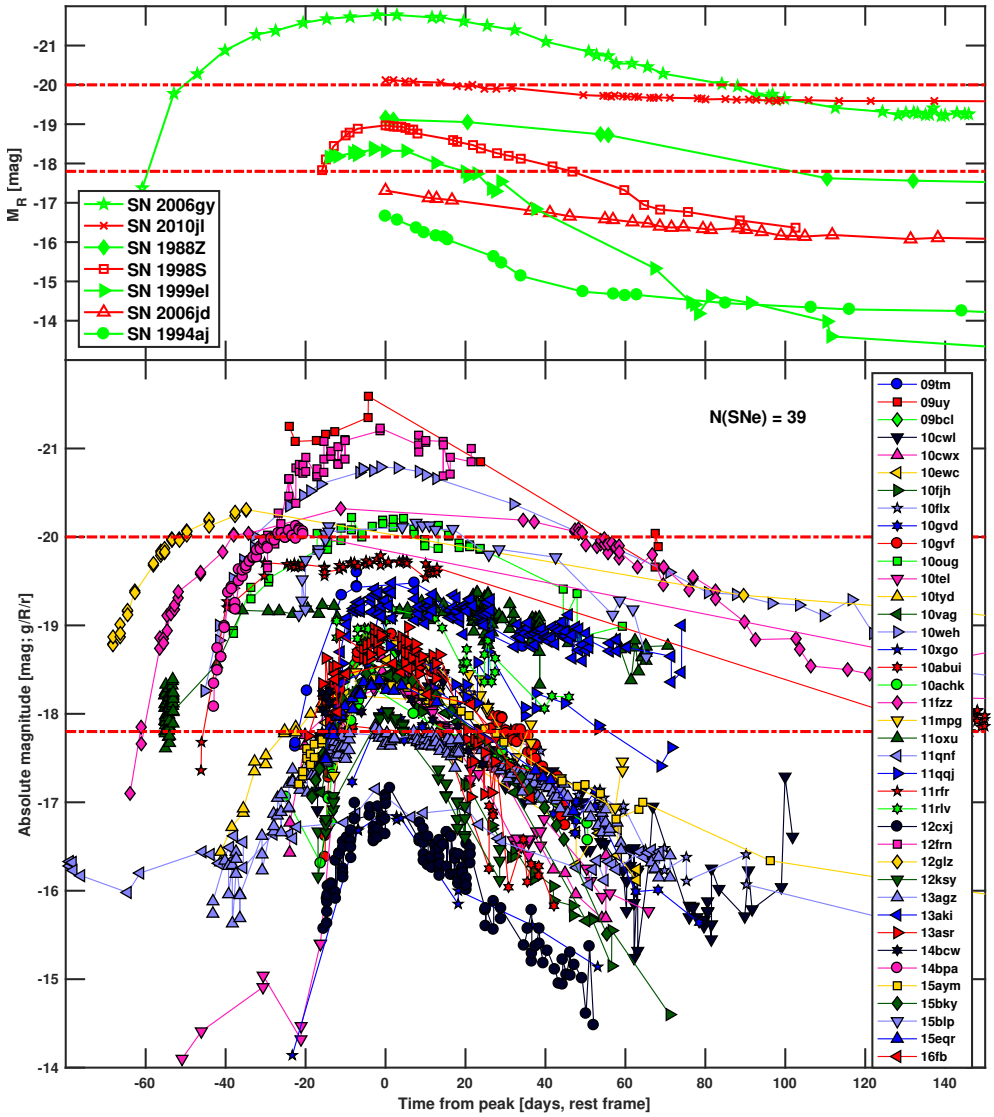

Figure 7. The bottom panel shows LCs of an untargeted sample of spectroscopically classified Type IIn SNe given in Nyholm et al. (2020). Red dashed lines represent the 1 σ variation in the peak magnitudes. The large variation in both the peak luminosity of the events and the evolution in time is clear. Top panel: LCs of a selection of well studied events, with the same 1 σ variation shown.

the SN ejecta, and this can produce strong X-ray emission (see e.g. Svirski & Nakar, 2014) or an early excess in the UV (Gezari et al., 2015).

As the SN ejecta expand, they collide with the CSM. The expanding ejecta are moving at $\sim 10^4$ km s^{-1}, while the CSM is moving only at $\sim$10-100 km s^{-1}, and their collision generates a pair of shocks. A forward shock propagates into the CSM, while a reverse shock propagates inward (in mass coordinates) into the SN ejecta (e.g. Fransson, 1982; Nadezhin, 1985; Chevalier & Fransson, 1994). Radiation from the forward shock will ionise some quantity of CSM ahead of it and at early times and for sufficiently dense CSM, the electron scattering photosphere can be outside of the shock interface (in region 1 of Fig. 8). This produces the blue continuum and Lorentzian wings for the narrow lines mentioned above, that characterise Type IIn SNe (see e.g. Smith, 2017).

As the density in the outer unshocked CSM decreases, we see through it to the shock interface. In between the shocked CSM and shocked ejecta, if the CSM is sufficiently dense, material can pile up to form a "cool dense shell" (CDS) (e.g. Chevalier, 1982; Chevalier & Fransson, 1994). This can be opaque, and in this case all spectral lines from the SN ejecta can be obscured behind the photosphere that resides in the CDS (Chugai et al., 2004). This can explain the blue continua and lack of broad absorption lines observed in e.g. SN 1998S (Leonard et al., 2000). Additionally, we can observe intermediate−width emission features, produced by post−shock CSM, that exists in a narrow layer outside of the CDS (Chugai et al., 2004). The strength and timescale of these effects depend on the density and extent of the CSM. If the interaction is short-lived, the emission from the CSM can decline and we can observe the photospheric or tail phase of the SN ejecta underneath, with only weak signatures of the CSM. This is the case for SN 1998S, which transitioned to show a photospheric spectrum within a few weeks of peak (Leonard et al., 2000). However, if the interaction is strong it can dominate the emission for years, and the underlying SN ejecta signatures can remain obscured, such as in the case of SN 2010jl (Fransson et al., 2014).

Interaction additionally generates emission through non-thermal processes. Synchrotron emission is produced by relativistic electrons in a magnetic field, and this process is observed in radio emission from interacting SNe. The conditions for this are created by the shocks present in the interaction region, which accelerate particles and amplify the magnetic field. The physics of this are not fully understood (see Caprioli & Spitkovsky, 2014a,b,c, for detailed analysis). Radio emission exhibits a characteristic wavelength-dependent "turn-on", which is due to the expansion of the emitting region causing decreasing absorption of the emission (Chevalier, 1982). The absorption can be a result of free-free processes, which will take place in the surrounding gas; or synchrotron self-absorption, in which the same electrons that emit the photons also absorb them.

Type IIn SNe are connected clearly to interaction through their definition, but

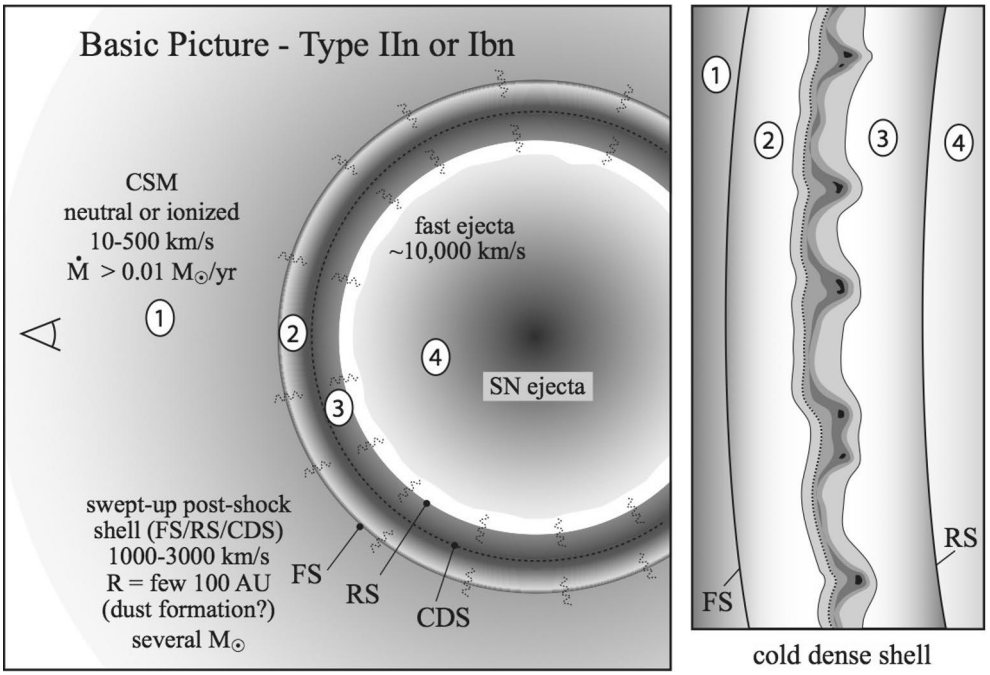

Figure 8. A schematic picture of spherical interaction in an interacting SN, taken from Smith (2017). The numbers label:

1. The unshocked, photoionised CSM.
2. The CSM that has been swept up after collision with the forward shock.
3. SN ejecta that are decelerated after collision with the reverse shock
4. The expanding SN ejecta that has not yet encountered dense CSM.

many other SNe that are not classified as Type IIn show signs of CSM interaction. Perhaps the most striking example is the famous peculiar Type IIP SN 1987A, which as the most recent nearby SN was observed at a spatial resolution far superior to all others. For this SN, HST imaging resolved an equatorial ring of CSM material at $\sim$ 0.6 light year distance from the progenitor, that was ionised by the shock breakout with a light travel time delay of $\sim$200 days, as well as two co-axial rings $\sim$1 light year above and below the plane of the inner ring (see McCray & Fransson, 2016, and refs therein). A few years after the explosion the collision between the SN ejecta and the equatorial ring was observed, and intermediate width spectral features from the shocked gas can be seen (Gröningsson et al., 2008). This highly non-spherically symmetric configuration of CSM indicates that the spherical model of Fig. 8 is likely not applicable for many SNe, and this is supported by observations with the HST which resolve CSM systems of nearby stars, and reveal asymmetrical CSM (see e.g. Humphreys et al., 1997; Smith et al., 2001).

There is evidence that the presence of CSM could be the cause of the different LCs of Type IIP and IIL SNe. Morozova et al. (2017) find from modelling that dense CSM close to to RSG progenitor can reproduce the LCs of Type IIL, and notably find that Type IIP LCs show evidence for this as well. Hillier & Dessart (2019) find similar results, with more linear SNe with brighter peak luminosities requiring more CSM to be well fit by their models. This theoretical work is supported by observational evidence for CSM interaction in Type IIL SNe, such as SN 2014G which showed evidence in its spectra for asymmetrical CSM (Terreran et al., 2016), and ASASSN-15oz, which showed evidence for CSM in the radio (Bostroem et al., 2019).

As noted above, Fig. 5 shows LCs of Type II SNe, and in particular highlights a group of SNe that have linear LCs but are more luminous than typical. These objects include SN 1998S, which is a well studied Type IIn SN, but also include a number of SNe such as SN 2013fc (Kangas et al., 2013) which are not classified as Type IIn SNe. These objects have peak magnitudes of $\sim$-20 mag, quite similar to Type IIn SNe such as SN 2010jl, although SN 2008es (Gezari et al., 2009a) has a similar decline rate but is much more luminous. Additionally, these events have spectroscopic features in common, as shown in Fig. 6. Absorption components of the Hα P-Cygni profiles of these objects are weak or not at all present, a feature they share with SN 2014G, a less luminous Type IIL. This group of objects has been considered a transitional group between Type IIP/L SNe, in which the influence of CSM interaction is low, and true Type IIn SNe, with strong interaction (e.g. Smith et al., 2015).

Dessart et al. (2016) suggests a model for SN 1998S in which a 10 $M_{\odot}$ ejecta collides into an extended CSM produced by a 0.1 $M_{\odot}$ yr^{-1} wind lasting for 3.5 years to explain the observed features. In Smith et al. (2015), a model making use of a disk configuration of CSM is used to explain the presence of CSM signatures at

early and late times, as well as the multi-component profile in the Hα emission lines (Leonard et al., 2000). A similar scenario without spherical symmetry is suggested in Paper II for SN 2016gsd, in which the presence of high velocity material at late times suggests directions through which SN ejecta can freely expand.

There are a number of mechanisms for generating CSM around stars. It is well understood that massive stars have a strong stellar wind, produced as UV photons emitted at the photosphere are absorbed or scattered by metals in the outer stellar material, and accelerate them (Lucy & Solomon, 1970; Castor et al., 1975). Massive stars have high enough luminosity that this mass loss can be large enough to influence the internal structure and evolution of the star throughout its time on the main sequence (see e.g. Chiosi & Maeder, 1986; Langer, 2012) and leave a significant quantity of material around the star. It is understood that these winds are "clumpy" (see e.g. Dessart & Hillier, 2005; Feldmeier, 1995; Owocki & Rybicki, 1984). This is due, among other reasons, to the effect of line-driven instabilities, caused by the velocity dependent nature of the line driven acceleration.

Stellar winds of the 8-16 $M_{\odot}$ RSG progenitor stars of Type IIP SNe are expected to produce mass loss rates of up to $\sim 10^{-4}\ M_{\odot}$ yr^{-1}, based on both observations of these stars (e.g. de Jager et al., 1988) and theoretical predictions (e.g. Castor et al., 1975; Vink et al., 2001; Beasor et al., 2020). Studies have found radio and X-ray emission detected in Type IIP SNe to be consistent with somewhat low mass loss rates of e.g. $10^{-6} M_{\odot}$ yr^{-1} (e.g. Chevalier et al., 2006). Some of the earliest well-observed radio SNe were the bright Type IIL SNe 1979C and 1980K Weiler et al. (1986). Modelling of the radio emission from these objects (Lundqvist & Fransson, 1988) implied mass loss rates of $\sim 10^{-5} - 10^{-4} M_{\odot}$ yr^{-1}, consistent with the upper end of the estimates for mass loss from stellar winds.

Some Type IIn SNe, such as SN 2010jl (Fransson et al., 2014), SN 1988Z (Aretxaga et al., 1999a), and SN 2015da (Tartaglia et al., 2020) exhibit the characteristic narrow line with broad wings for a year or more, and are considerably more luminous than normal SNe, with long lasting LCs. These SNe require episodic mass loss with much higher mass loss rates of $\sim 0.1 M_{\odot}$ yr^{-1} and CSM velocities of $100-1000$ km s^{-1} to generate the density of the CSM required to explain their observable characteristics, and this is often attributed to eruptions of Luminous Blue Variable stars (LBVs). LBVs are observed to have violent mass loss histories, with η Carinae in the Milky Way having a long and well observed history of variability (Smith & Frew, 2011) combined with an observable $10-20\ M_{\odot}$ of CSM containing 10^{50} ergs of kinetic energy (Smith et al., 2003). These eruptions are observed as "supernova impostors", luminous transient events which have characteristic velocities of 100-1000 km s^{-1} and eject 0.01-10 $M_{\odot}$ (Smith et al., 2011a), consistent with measurements of CSM from Type IIn SNe such as 2010jl. Such eruptive mass loss events are postulated to be caused by a sudden increase in luminosity in the star that then drives an extremely strong stellar wind (Humphreys & Davidson, 1994; Shaviv, 2000; Smith

& Owocki, 2006). However, questions such as the exact cause of the increase and whether it can replicate the wind velocities observed are unanswered (see e.g. Smith et al., 2011a). The progenitor of the Type IIn SN 2005gl was identified as an LBV (Gal-Yam & Leonard, 2009), providing evidence that LBVs can produce these SNe.

Another major component of the mass loss history of a star is the influence of a companion star. As mentioned in Sect. 2.1, it is estimated that at least 50%, and as many as 70% of massive stars exist in binary systems, and will interact in some form in their lifetime (Mason et al., 2009; Sana et al., 2011, 2012), so we expect to see the influence of this interaction in many CCSNe that we observe. Within binary star systems, one can consider a surface known as the "Roche lobe" within which material is gravitational bound to a particular star within that system. Massive stars will increase in radius during their lifetimes due to changes in the nuclear burning processes and internal composition of the star and thus their envelopes can expand outside of the Roche lobe. This "roche lobe overflow" (RLOF) will cause mass from the expanded star to accrete onto the companion. This can drastically change the composition and evolution of both objects. The donor star can potentially lose some or all of its H envelope, and then some or all of its He envelope, depending on the degree of RLOF and evolution of the binary system. These scenarios have been connected to Type IIb SNe in the case of partial H stripping (Maund et al., 2004; Fox et al., 2014), and Type Ib and Type Ic SNe in the case of full H or full He stripping respectively (see e.g. Langer, 2012).

In less extreme cases, a star could experience RLOF and then still explode as a H−rich SN (as opposed to Type IIb which have very low mass H envelopes at explosion (see e.g. Ergon et al., 2015)). The accreting star, or "mass gainer", in the binary will typically be the less massive member, and thus be more slowly evolving and still on the MS when the accretion occurs. Such a relatively unevolved star is expected from calculations to be capable of incorporating the new mass and evolving similarly to a star with ZAMS mass similar to the accreting stars new mass (Hellings, 1983, 1984; Braun & Langer, 1995). Compared to a single star with the same ZAMS mass as the gainer's post-accretion mass, a mass gainer will have higher angular momentum and a longer lifetime. Smith & Tombleson (2015) argues that mass gainers could be progenitors for LBVs as this could explain their isolated positions away from young stars as they would have longer lifetimes and could experience natal kicks from their birthplace when their initially higher mass companion explodes. The enhanced rotation of mass gainers would help to explain LBV eruptions.

The endpoint of binary interaction in some cases will be a merger. Stars can merge either while they both are on the main sequence, when one has evolved a compact H-depleted core, or when both stars have evolved such a core. Mergers of binary systems have been suggested to make up a significant proportion of all Type II SN progenitors, with Zapartas et al. (2019) finding the figure to be 31^{+13}_{-19}% from numerical population synthesis simulations. The progenitor of SN 1987A was sug-

gested to be a post merger product, due to the presence of CSM, as well as surprising blue color and He-rich envelope (e.g. Podsiadlowski, 1992; Vanbeveren et al., 2013). Simulations by Morris & Podsiadlowski (2007) found that this scenario could also reproduce the triple ring structure of CSM observed during the SN. However, an LBV scenario has also been invoked for SN 1987A, particularly by comparison to observed LBVs with a similar triple ring structure (Smith, 2007).

2.3.3 Supernovae in luminous infrared galaxies

Understanding SN rates is crucial for constraining our theories of stellar evolution. Establishing volumetric rates of CCSNe can precisely determine their relative rate compared to the star formation rate (SFR), allowing a measurement of the quantity of stars that end their lives as SNe. This can, among other things, constrain the number of failed SNe (described above in section 2.2.2). Horiuchi et al. (2011) compared the most recent SN rate measurements of the time with the SFR, both as a function of redshift. They found that the prediction for the SN rate from the SFR was approximately double that inferred from observations made by surveys at all redshifts apart from the very local volume (where other authors (Botticella et al., 2012) found good agreement). This implied that large quantities of stellar deaths were not being observed, and the authors suggested that these SNe could be "dim" either due to being intrinsically faint (perhaps failed SN) or obscuration by dust. To distinguish between the possible explanations for this discrepancy, one must consider locations where large quantities of obscured SNe can take place, which requires both significant star formation to yield a high SN rate, and the presence of dust that can cause obscuration. Galaxies which fit both these criteria are luminous infrared galaxies (LIRGs).

LIRGs (see Fig. 9) are defined as galaxies that have infrared (IR, here defined as 8-1000 μm) luminosity $L_{IR} > 10^{11} L_{\odot}$, with ultraluminous infrared galaxies (ULIRGs) having $L_{IR} > 10^{12} L_{\odot}$ (Sanders et al., 2003). These galaxies are more luminous in the IR than at all other wavelengths combined, and many of them were not classified until the Infrared Astronomical Satellite (IRAS) all-sky IR survey in the 1980s, having been previously missed by optical surveys (see e.g. Wright et al., 1984; Houck et al., 1985). The strong IR emission in LIRGs is due to radiation from warm dust, which is heated either by emission originating from accretion onto a central SMBH (an active galactic nucleus (AGN), see Sect. 3.1); UV emission from hot, young, massive stars created during recent star formation; or a mixture of both (Pérez-Torres et al., 2021).

The SFR in LIRGs is high: assuming a Salpeter IMF, solar metallicity and a continuous burst of star formation over the last 10-100 Myr, Kennicutt (1998) finds

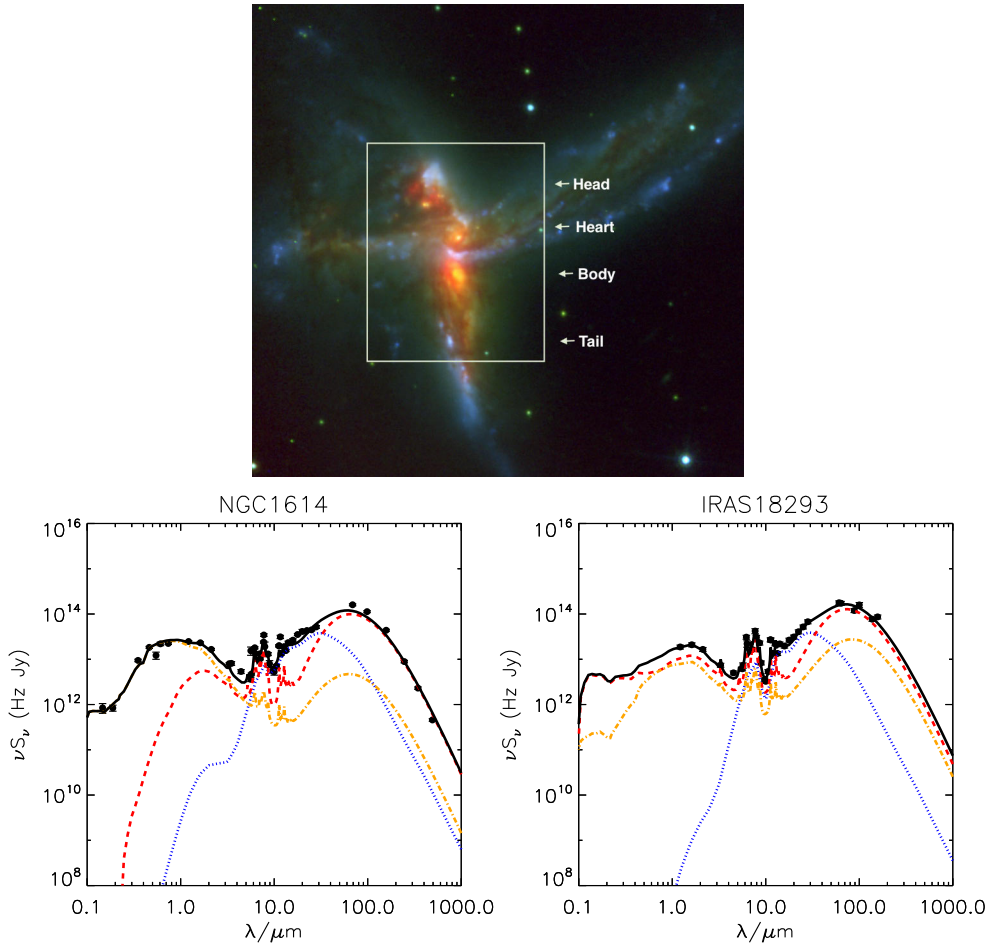

Figure 9. Top: A three-colour image of the LIRG IRAS 19115-2124, known as "The Bird", combining K, I and B-band observations. The main components of the galaxy are labeled. Taken from Väisänen et al. (2017). Bottom: Spectral energy distributions of 2 LIRGs (black points), along with fits using radiative transfer models (solid black line). The starburst component (red), AGN torus (blue) and spheroidal host (orange) of the fit is shown. The starburst component contributes significantly to the IR luminosity of the LIRGs. Taken from Kankare et al. (2021).

the implied SFR as a function of L_{IR} is:

$$\text{SFR} \sim 17.3 \left(\frac{L_{IR}}{10^{11} L_{\odot}} \right) \text{M}_{\odot} \text{ yr}^{-1} \tag{5}$$

which is significantly higher than, e.g., the Milky way SFR which is $\sim$2 $M_{\odot}$ yr^{-1} (Chomiuk & Povich, 2011). LIRGs are relatively rare in the local universe, but become more common moving out to redshift z$\sim$1, where they dominate the SFR (Magnelli et al., 2009, 2011). The high SFR in these galaxies implies a large CC-SNe rate: as more massive stars live for shorter periods, and these are the stars that undergo CCSNe, CCSNe are strongly correlated with recent star formation. Therefore, in order to infer the volumetric SN rate accurately at the higher redshifts where LIRGs dominate the star formation, it is required to detect and study SN occurring within local LIRGs.

Optical surveys often fail to detect SNe within LIRGs. Mattila et al. (2012) used the case study of the nearby LIRG Arp 299 to estimate the rate at which CCSNe were being missed in LIRGs, finding that 83^{+9}_{-15}% of SNe had been missed by optical searches in the 14 year period before the publication of their work. The difficulty in detecting these SNe in optical observations lies both in their proximity to the nucleus and their higher than average extinctions. Star formation in LIRGs is concentrated in nuclear regions (e.g. Soifer et al., 2001), where high spatial resolution not typically used in surveys is required to detect transient objects against the complicated galaxy background. The dust present in LIRGs can extinguish SNe by at least a few magnitudes in the optical (Pérez-Torres et al., 2021), where the effect of dust extinction is strong, making them faint enough to be missed by surveys.

To detect SNe in LIRGs, observations can be performed in the IR, where the effect of dust extinction is much less. Such observations have detected multiple SNe in LIRGs (see e.g. Mattila & Meikle, 2001; Maiolino et al., 2002; Mannucci et al., 2003; Miluzio et al., 2013; Jencson et al., 2019; Kankare et al., 2021; Fox et al., 2021), including some that have large extinctions (e.g. Kankare et al., 2014; Kool et al., 2018) with the most extreme being SN 2008cs (Kankare et al., 2008), which had a host extinction in V-band of $\sim$16 magnitudes. Additionally, observations in radio can even more effectively see through the dust, suffering no extinction, and CCSNe emit in radio both during their terminal explosion through their interaction with CSM as described above in Sect. 2.3.2, and later on as SN remnants, where the expanding SN ejecta interacts with dense interstellar material (Chevalier & Fransson, 2001). A number of studies of Arp 299 with high resolution radio telescope networks (Pérez-Torres et al., 2009; Ulvestad, 2009; Bondi et al., 2012) have revealed dozens of compact sources, attributable to SNe or SN remnants, that have been used to infer a CCSN rate $>$0.8 yr^{-1}.

By factoring in the population of SNe that are going unobserved in LIRGs, Mattila et al. (2012) found that the discrepancy noticed by Horiuchi et al. (2011) between

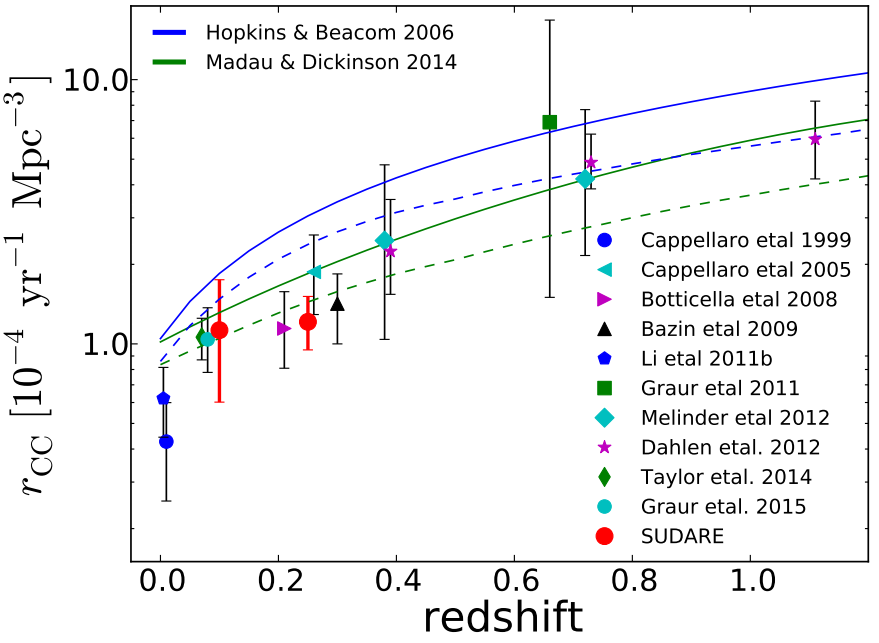

Figure 10. A compilation of measurements of the CCSN rate per unit co-moving volume, taken from Cappellaro et al. (2015). The solid lines show the predictions from a Salpeter IMF with the range 8-40 $M_{\odot}$ adopted for core-collapse progenitors. The dashed lines show the effect of the correction of Mattila et al. (2012), which improves the agreement with CCSN rates at low and intermediate redshift. At higher redshifts the large statistical and systematic uncertainties make an agreement between the SFR and SNR hard to verify.

the SN rate and SFR can be resolved (see also Mannucci et al., 2007; Dahlen et al., 2012; Madau & Dickinson, 2014; Strolger et al., 2015). However, as noted by Cappellaro et al. (2015), the measurements of SNR and SFR, as well as the mass range of SN progenitors, still have both statistical and systematic uncertainties that make it difficult to assess whether the SFR and SNR agree, particularly at high redshifts (see Fig. 10). Further work to identify the intrinsic rate of SNe in LIRGs is described in Paper III, in which near-infrared (NIR, here defined as $\sim$1 - 2.5 μm) adaptive optics (AO) observations are used in order to discover SNe close to the nuclei of LIRGs.

3 Transients related to supermassive black holes

The majority of the galaxies in the local universe host a SMBH, defined as a BH with M_{BH} >10^6 $M_\odot$, at their centre (see e.g. Miller et al., 2003). These SMBHs are a potential source of large amounts of energy. If a body of mass m falls onto a body of radius R and mass M, the gravitational potential energy released is $E_{grav} = GMm/R$, where G is the gravitational constant. If we compare this to the rest mass energy of the body, $E_{rest} = mc^2$ we can consider the accretion efficiency:

$$\eta_{acc} = \frac{GMm/R}{mc^2} = \frac{GM}{Rc^2} = \frac{R_s}{2R} \tag{6}$$

where $R_s = \frac{2GM}{c^2}$ is the Schwarzschild radius, the location of a BHs event horizon. This efficiency can be very high. For example, typical values for the mass and radius of a NS yield $\eta_{acc} \sim 0.1$. In this case, it can be assumed that when the material collides with the solid surface, all of its kinetic energy is converted into thermal and radiated energy. However, for a BH there is no such solid surface, and in order for us to observe it, the kinetic energy of the accreting material must be converted to radiation before it passes the event horizon. For a Schwarzschild BH, the innermost stable orbit can be estimated with a pseudo-Newtonian approach (see e.g. Frank et al., 2002, for a derivation) as $R_{min} = 6GM/c^2 = 3R_s$. Once material passes this radius, it falls quickly past the event horizon and we can assume any energy is lost inside the BH. Therefore the maximum available energy that can be radiated is the binding energy at the innermost stable orbit, which is $(GMm/2R_{min})$. This implies that $\eta_{acc} = 1/12$ for a BH in the Newtonian approximation[1](Frank et al., 2002).

These efficiencies are very high: the efficiency of nuclear H burning is only 0.7%, an order of magnitude less. If a SMBH is spinning, the innermost stable orbit can be much closer, yielding efficiencies up to $\sim 40\%$. Whether the kinetic energy of accreting material is released as radiation before it passes the event horizon depends on the geometry of the accretion. If the accretion is spherical, a situation known as Bondi accretion, the ratio of radiated energy to rest mass energy of accreted material can be estimated as only $\sim 10^{-4}$, much less than η_{acc} (see e.g. Netzer, 2013). However, if the material instead forms an accretion disk, then this ratio is expected

[1] A calculation treating relativity fully gives $\eta_{acc} \sim 6\%$ (Netzer, 2013)

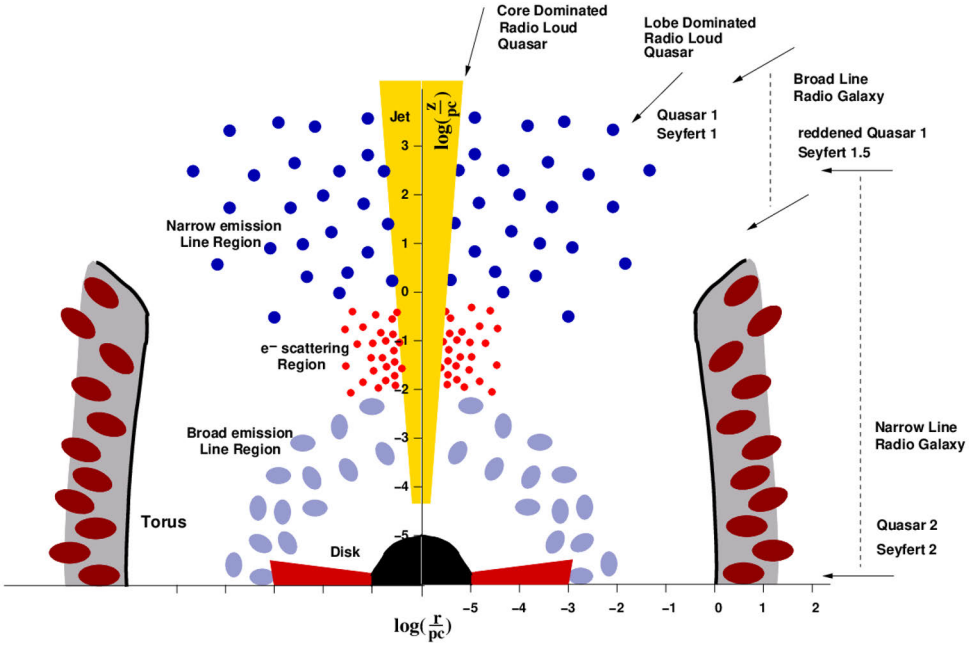

Figure 11. This figure from Zier & Biermann (2002) shows a schematic representation of an AGN. The central SMBH is shown in black, and the other major AGN structures are labelled. The axes are logarithmically scaled to 1 pc, and show the approximate sizes of these structures. The lines of sight associated with various AGN types are labeled and shown with black arrows.

to be much higher, as the viscosity in the disk can transport angular momentum of infalling material outwards, and the slowly in-spiralling material has time to radiate much more of the released gravitational potential energy (see Shakura & Sunyaev, 1976, for a seminal treatment of accretion disks).

3.1 Active galactic nuclei

The most commonly observed phenomena associated with accretion onto a SMBH is that known as an AGN. An AGN is defined generally, as a galaxy nucleus that emits more strongly than a "typical" galaxy nucleus, which can be caused by a variety of potential physical processes. AGN are common, with $>20\%$ of SMBHs residing in an AGN (Miller et al., 2003). Despite the variety of observed features, a unified model to explain them in terms of simple parameters was produced by Antonucci (1993). A schematic of this model is shown in Fig. 11, and I will briefly describe the main observational features associated with it, drawing primarily from Netzer (2013) as a reference.

Close to the SMBH, at sub-pc scales, a rotating accretion flow forms, usually

termed the accretion disk. This accretion disk is hot, reaching temperatures of up to 10^5 K (e.g. Netzer, 2013), and produces an observable "blue bump" in the spectral energy distribution (SED) of the galaxy (see e.g. Sanders et al., 1989). Slightly further out, gas orbiting the SMBH is ionised by the radiation from the accretion and produces broad (a few 1000 km s^{-1} (Padovani et al., 2017)) recombination lines, with the breadth coming from Doppler broadening. The region where this gas resides is termed the "broad line region" (BLR). Further out, lower density gas is also ionised, but due to its distance from the SMBH and corresponding lower velocity, the emission lines associated with it are much narrower (300-1000 km s^{-1} (Padovani et al., 2017)) leading to it being termed the "narrow line region" (NLR).

The key feature of the unified model is that the angle from which we observe the AGN will determine what we observe. The accretion onto the central SMBH is (approximately) axisymmetric, and a viewing angle along the polar axis provides an unobstructed view to the central regions, where we see the accretion disk and the BLR. The unified model suggests that there exists a "dusty torus", consisting of a clumpy distribution of molecular and atomic gas, with a large opacity, which completely obscures the central regions of the AGN in the equatorial directions (Ramos Almeida & Ricci, 2017). When observing from directions obscured by the torus, the NLR can be seen, but the BLR and accretion disk are obscured. The polar viewing angle corresponds to Type 1 AGN, defined as those we see which exhibit broad lines, and Type 2 AGN, those without. Key evidence that motivated this scheme was the observation of broad lines in the polarized spectra of Type 2 AGN, which in the unified model are explained as obscured BLR features scattered into the line of sight (LoS) by free electrons and dust in the polar regions above or below the accretion disk that are unobscured by the dusty torus (Antonucci & Miller, 1985; Smith et al., 2002).

Another major way that AGN are classified is based on the presence or absence of radio emission. Around 10% of AGN are "radio-loud", strong radio sources, and this led to most of the first known AGN being discovered in radio. Most radio emission from AGN shows a synchrotron power−law continuum, indicating the presence of relativistic electrons in a magnetic field. Also observed are large resolved structures of radio emission, which extend out along one or both directions of the polar axis. These can extend out to 1 Mpc from the SMBH (Blandford et al., 2019), covering a much larger scale than e.g. the $\sim$ 1-10 pc dusty torus within the AGN (Ramos Almeida & Ricci, 2017). These characteristics and more point to the presence of jets, large outflows of energetic particles launched from close to the SMBH. These jets can approach relativistic velocities which creates another viewing angle dependent characteristic: when viewing close to the jet axis, relativistic beaming in the jet produces extremely luminous sources, such as blazars (see e.g. Blandford et al., 2019).

An important feature of AGN is that many of them are variable. Most Type 1

AGN exhibit optical variability, particularly in bluer bands, on a variety of timescales from hours to years (see e.g. Vanden Berk et al., 2004; Ulrich et al., 1997). Typical variability is a few tenths of a magnitude in amplitude on timescales of months (MacLeod et al., 2016, 2012) but it can be multiple magnitudes (e.g. Valtonen et al., 2008). Lower amplitude variability is well modelled by a damped random walk, a stochastic process (Kozłowski et al., 2010; Kelly et al., 2009), and is associated with the accretion disk, perhaps arising from instabilities or structural changes in the disk, but this is not fully understood (see e.g. Dexter & Agol, 2011; Kokubo, 2015). This stochastic variability extends into other wavelengths, with variability being typically faster at shorter wavelengths (e.g. X-rays). Larger changes in magnitude can be associated with relativistic jets, and is often seen in blazars (see e.g. Ulrich et al., 1997). IR variability has been observed to experience time lags compared to the optical variability of the same AGN (Koshida et al., 2014). The IR light is produced by the inner parts of the dust torus, which are heated by the optical flare. The time delay corresponds to the time taken by light to travel from the accretion disk to the torus, and thus can be used to measure the size of the torus (see e.g. Clavel et al., 1989; Koshida et al., 2009; Lira et al., 2011). The IR variability can evolve over timescales of years to decades (Kozłowski et al., 2016). Radio variability is thought to be associated with variations in the jet. Type 2 AGN typically are not variable in UV and X-ray, as the accretion disk and regions around it which produce variability are obscured, but AGN with weak broad components can shown variability (Hernández-García et al., 2017).

As well as the "typical" variability seen in many Type 1 AGN, there are additionally AGN that undergo larger and more structured variation. There have long been known to be examples of AGN that transition from Type 1 to Type 2, or vice−versa (e.g. Khachikian & Weedman, 1971; Penston & Perez, 1984; Aretxaga et al., 1999b). This group of objects, known as "changing-look AGNs" (CLAGNs), could be in tension with the unified model, as neither the orientation or viewing angle of the AGN can change. A suggested explanation is that variable extinction along the LoS to the BLR, due to orbiting dust or gas clouds moving into it, could lead to these transitions (see e.g. Goodrich, 1989a; Tran et al., 1992), but there is doubt that such material could exist at the required position (see e.g. Nenkova et al., 2008a,b) and at least one example exists where this explanation fails (LaMassa et al., 2015). An alternative explanation is a change in the level of ionising flux produced from the central regions, likely due to a change in the accretion rate. MacLeod et al. (2016) performed a systematic search for CLAGNs, and found that all of those they found experienced a large change in g−band continuum flux accompanying the change in spectral features, with an >1 mag increase associated with lines appearing and vice versa.

Additionally, there have recently been a number of optical flares observed in AGN without the associated change in AGN spectral type which do not appear to

be consistent with previously known forms of AGN activity. These include events such as PS1-10adi, (Kankare et al., 2017), PS16dtm (Blanchard et al., 2017) and family of new discoveries arising in recent surveys (Lawrence et al., 2016; Graham et al., 2017; Frederick et al., 2020) among others. A number of these transients have been associated with a type of AGN known as narrow-line seyfert 1 galaxies, which show, among other features, narrower broad lines than typical for a Type 1 AGN ($<$2000 km s^{-1}) (Osterbrock & Pogge, 1985; Goodrich, 1989b) and are associated with smaller SMBHs with high accretion rates (see e.g. Boller et al., 1996; Rakshit et al., 2017). A number of origins for these flares have been suggested such as changes in accretion rate of the SMBH (Trakhtenbrot et al., 2019), microlensing of AGN by a foreground source (Lawrence et al., 2016), superluminous SNe (Graham et al., 2017), tidal disruption events (Blanchard et al., 2017; Tadhunter et al., 2017), or specifically SNe or tidal disruption events that interact with their ambient medium (Kankare et al., 2017).

3.2 Tidal disruption events

An additional method of harnessing the power of accretion is for a star to be accreted onto a BH. If a star approaches close enough to a SMBH, it may pass through its Roche limit, the point at which the tidal force it experiences due to the BHs gravity is larger than the stars internal gravitational binding force, causing it to become unbound. This is known as a tidal disruption event (TDE). The radius this occurs at is approximately[2] (Hills, 1975):

$$R_T = R_* \left(\frac{M_{BH}}{M_*} \right)^{1/3} \tag{7}$$

where R_* and M_* are the radius and mass of the star, and M_{BH} is the BH mass. For the signatures of the disruption to be visible to an observer, this radius must be larger than the event horizon of the BH. For a non-rotating (Schwarzschild) BH, this lies at R_s. As R_s increases with mass, this implies that there is an upper mass limit for SMBHs that can visibly tidally disrupt a star, known as the "Hills mass": $M_{\rm Hills} \sim 10^8\ M_\odot$ (Hills, 1975). However, for a rotating BH (known as a Kerr BH, (Kerr, 1963)), this limit can be higher (Kesden, 2012).

The situation once the star is torn apart is shown in Fig. 12. The stellar material is spread over a range of energies/velocities causing $\sim$ half of it to escape the gravity well of the SMBH, while the rest begins to spiral inwards (Rees, 1988). This is due to the difference in gravitational potential across the star at the point it crosses the

[2]This equation neglects the star's rotation and general relativistic effects, among others, but these effects are captured in an order unity factor that lies within the cube root, so the equation is quite accurate. If $R_T \sim R_s$, general relativistic effects can not be neglected and the SMBH spin and orbital inclination of the star are important. See Rossi et al. (2021) and refs therein for more details.

Roche limit which leads to a large dispersion in velocities for the stellar material post-disruption (Lacy et al., 1982). The bound material will then spiral inwards towards the BH. Making some simple assumptions about the material, it can be shown that the expected rate it returns to the BH is $\propto t^{-5/3}$ (Rees, 1988; Phinney, 1989; Evans & Kochanek, 1989). If we assume the accretion luminosity is proportional to this rate then the LC of a TDE would also follow the same behaviour over time. More recent work has shown that the assumptions are not generally valid, and that this rate will only hold a few months after the disruption, while the density structure of the star will strongly influence the fallback rate at earlier times (see e.g. Lodato et al., 2009; Lodato & Rossi, 2011; Guillochon & Ramirez-Ruiz, 2013). Fig. 12 shows a very shallow angle of approach for the star towards the SMBH, but this need not be the case. The star could also approach the SMBH very directly, at any angle in between, or not quite reach the Roche limit and be partially disrupted, affecting the properties of the TDE event that results (e.g. Carter & Luminet, 1983; Stone et al., 2013; Gafton & Rosswog, 2019).

Some time after the publication of theoretical papers predicting the TDE phenomena (i.e. Rees, 1988, and others cited above) came the detection of TDE candidates. A major hurdle in unambiguously detecting TDEs is the ubiquitous variability of AGN nuclei at all wavelengths. Any transient detection in a galaxy with AGN signatures could potentially be due to variability in previously existing AGN structures, such as an accretion disk. The simplest way to distinguish a TDE from AGN activity is to only take candidates from quiescent galaxies, without a pre-existing accretion disk and lacking the characteristic emission lines of AGNs.

The first TDE candidates discovered were X-ray transients, discovered in the ROSAT all-sky survey (e.g Bade et al., 1996; Komossa & Greiner, 1999; Grupe et al., 1999; Greiner et al., 2000). Further candidates were found with new generations of X-ray facilities, and a few dozen have now been detected (Saxton et al., 2020). Some candidates, for which there were sufficient well sampled data, have shown the characteristic $t^{-5/3}$ decay rate for TDEs (e.g. Komossa & Greiner, 1999). There is notably a large variation in the properties of these events, in particular in their longevity, with most having quick decays of a few months to years, but a few events being longer lived, including an event that has lasted a decade (Lin et al., 2017), and a number of candidates for very fast events (see e.g Jonker et al., 2013). There are a number of possible explanations for these variations, such as a higher mass star (Lin et al., 2017) or larger circularisation of debris for longer lived events (Guillochon & Ramirez-Ruiz, 2015), or disruption by an intermediate mass BH with mass between 10^3 and $10^5 M_\odot$ for the short lived events (Jonker et al., 2013).

Later surveys extended the observations of TDEs across the EM spectrum. TDEs have been discovered in the UV (Gezari et al., 2006, 2008, 2009b) and later in optical surveys (van Velzen et al., 2011), greatly expanding the total number of discoveries. In recent times discovery rates have increased leading to the first sample studies

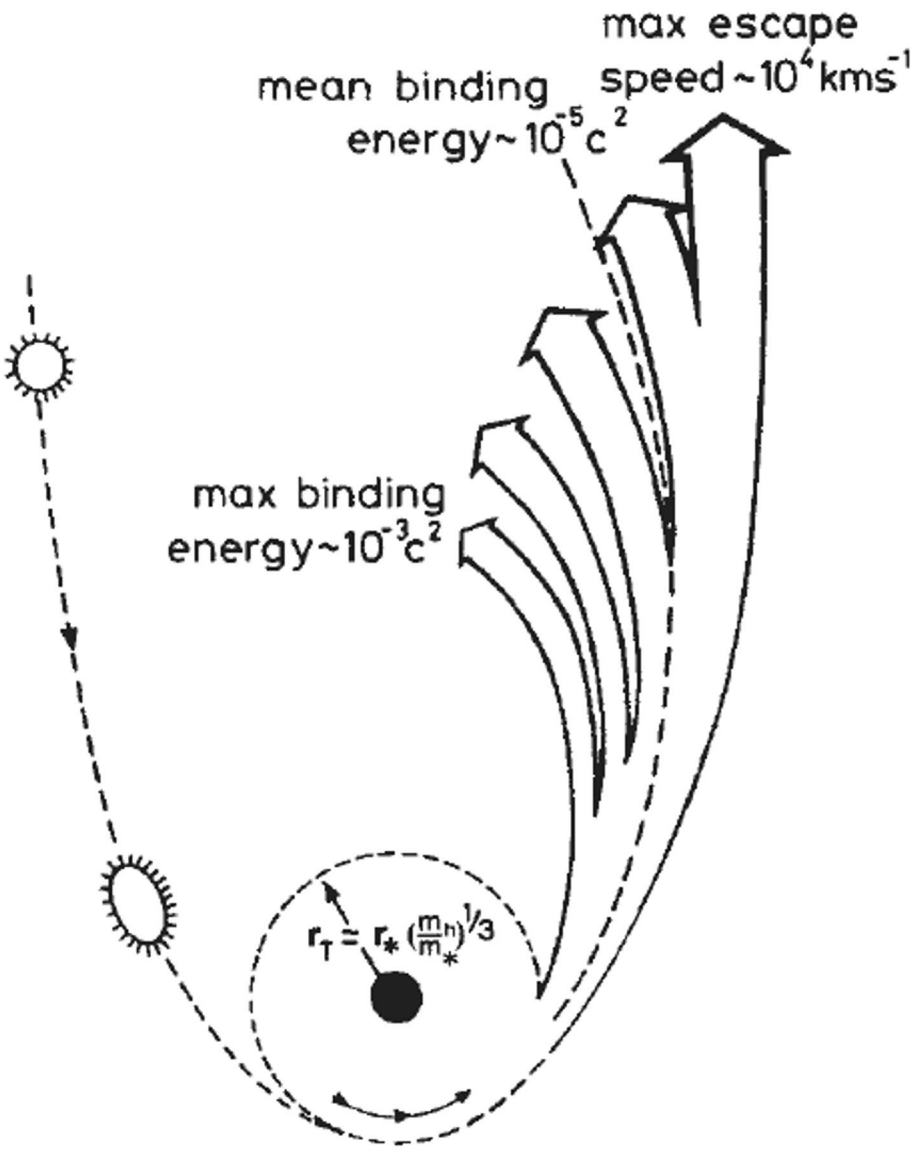

Figure 12. Figure from Rees (1988) that shows the tidal disruption of a star. The equation defines the radius at which a star will be disrupted, as described in the text. Approximately half the mass of the star is expected to escape while the rest remains bound and will accrete onto the BH.

(van Velzen et al., 2021). Characteristic properties of these UV/optically discovered TDEs include a hot spectral continuum with superimposed broad emission lines (5000-15000 km s^{-1}) as well as a fairly long rise time of weeks or months in optical photometry and a decline somewhat consistent with $t^{-5/3}$ (van Velzen et al., 2020; Gezari, 2021).

These TDEs have some observed features that challenge the models of the 80s. The UV/optical blackbody (BB) observed has a radius that is 2-3 orders of magnitude larger than the radius of the circularising debris from the TDE and is more luminous and cools more slowly than expected. This suggests the presence of a larger structure, which could be due to an outflow/wind (e.g. Miller, 2015; Metzger & Stone, 2017), or the intersection of the debris streams (e.g Piran et al., 2015; Bonnerot et al., 2017). The former case is supported by evidence for outflows seen in spectroscopy in optical, UV, X-ray and potentially radio wavelengths (see e.g. Miller, 2015; Alexander et al., 2016; Hung et al., 2019; Blagorodnova et al., 2019). In the latter case, it has been suggested that the formation of the accretion disk, rather than the actual accretion, could power the observed transient (Piran et al., 2015).

In spectroscopy there are emerging subclasses of optical TDEs. Events span a sequence between those with strong H emission (van Velzen et al., 2011), to those with no H and only He II emission lines (Gezari et al., 2012), with some events showing both, or even transitioning between the two states (Nicholl et al., 2019). Some events show O III λ3760 and N III λ4100 and λ4640 emission lines (e.g. Blagorodnova et al., 2019; Leloudas et al., 2019; Holoien et al., 2020), which are associated with the Bowen fluorescence effect (Bowen, 1934). The effect is produced by the de$-$excitation of fully ionised He to He II. The final transition, corresponding to He II Lyα, produces extreme UV photons at λ303 Å. These photons can produce excited states of O III, due to the O III transitions available at very similar wavelengths. The following de$-$excitation cascade produces the observed O III optical lines, and additionally produce an EUV photon at λ374 Å that can repeat the process through a resonance N III line. Bowen fluorescence was predicted to occur in SMBH accretion events by Netzer et al. (1985) and has now been observed both in TDEs as well as a new class of AGN accretion events/TDE candidates (Trakhtenbrot et al., 2019), that will be discussed further below.

A variety of explanations have been invoked for the different observed spectral characteristics, such as the chemical composition of the star (Gezari et al., 2012); ionisation conditions within the debris (Guillochon et al., 2014); and the viewing angle of the TDE (Nicholl et al., 2019), among others. van Velzen et al. (2021) sorts TDEs into TDE-H, TDE-He and TDE-Bowen based on the presence of these lines in spectra in the first spectroscopic sample study, and find correlations between these classifications and other features of the events, in particular the properties of the inferred BB associated with them.

The TDE detections described above in optical, UV and X-ray all observe emis-

sion expected to be associated with the accretion disk, although with the caveats mentioned above for optical emission. Emission at other wavelengths can arise from different structures, either associated with the TDE phenomenon or with surrounding material in the galaxy nucleus. Alexander et al. (2020) reports nine TDEs that have been detected in radio, while a few dozen others have published upper limits for non-detections. Some radio events, such as Sw J1644+57 (e.g. Zauderer et al., 2011) and Arp 299-B AT1 (Mattila et al., 2018), are powered by relativistic jets, launched from the TDE. When viewed on−axis, these jets produce very luminous emission due to the relativistic beaming effect. They contrast with radio TDEs such as ASASSN−14li which are 3 orders of magnitude less luminous. The emission from this object can be less unambiguously determined and has been suggested to arise from a non−relativistic outflow (Alexander et al., 2016), a sub−relativistic jet (van Velzen et al., 2016a) or the debris stream created from the unbound stellar material produced in the TDE (Krolik et al., 2016). The emission in many of these scenarios arises from the shock formed as the ejected material collides with the medium in the vicinity of the SMBH, and thus allows this material to be probed. Notably, not all TDEs are detected in radio, although it is not yet well understood which TDEs lacking relativistic jets will produce radio emission and which will not (see Alexander et al., 2020, for a recent review).

The final observations of TDEs I will describe are TDE detections in the IR. As the typical observed continuum emission from the TDE is hot (10000-40000 K; van Velzen et al. (2021)), it has a minimal contribution in the IR. However, the UV/optical emission can be absorbed by the dust in the vicinity of the SMBH and re-emitted at IR wavelengths. This phenomenon has been described in the context of AGN, where the presence of a dusty torus produces an observable NIR "bump" in AGN spectra (Barvainis, 1987), and the IR variability described in Sect. 3.1. It has also been observed in the SN context, where the SN light heats pre-existing dust in CSM (Graham et al., 1983; Dwek, 1983). The UV/optical emission will destroy dust heated to above a certain temperature, typically around 1500 K, depending on the composition of the dust (Barvainis, 1987; Guhathakurta & Draine, 1989). The temperature of a dust grain is determined by the equilibrium between the heating provided by the nuclear flare and the cooling due to radiation and sublimation (destruction) of the dust grain (see e.g. Lu et al., 2016). Dust will be destroyed out to some distance from the SMBH, depending on the luminosity of the flare and the dust sublimation temperature. The IR emission begins only once light travels out to this distance, and the light travel time creates a time−lag between the UV/optical flare and the rise of IR emission. As shown in Fig. 13, a simple model of this process, with some assumptions, can be used to infer properties of the dust in the SMBH environment given observations of the IR echo and optical flare. A luminous AGN can create a dust free cavity larger than the sublimation radius associated with a TDE, and in this case the time lag will not correspond to the luminosity of the TDE. These IR transients,

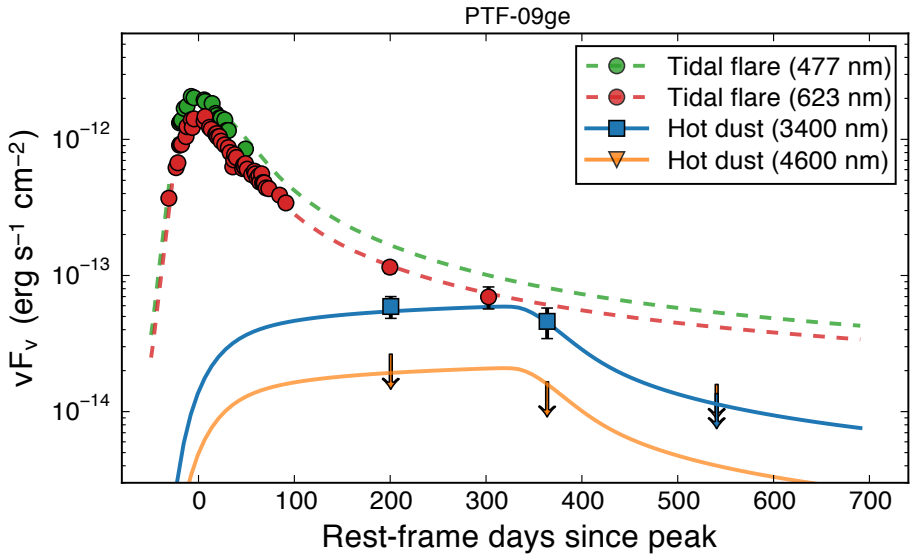

Figure 13. Figure taken from van Velzen et al. (2016b) that shows the optical (circles) and IR (squares and limits) flare associated with a TDE. The solid lines show the IR echo derived from the optical LC (the dashed lines) using a simple model in which the the optical flare is reprocessed in a thin dust shell with temperature T = 1850 K. The data are well fit by the model and the best fit parameters are a radius of 0.15 pc and covering factor of 0.01.

known as IR echoes, have been observed in a number of TDEs (van Velzen et al., 2016b; Mattila et al., 2018) as well as other nuclear transients and TDE candidates (e.g. Dou et al., 2017), and are a major subject of Sect. 3.3.

Observing the energy and timescale of these IR flares yields information on the UV/Optical flare as well as the environment of the nuclear regions. In particular, they present a possibility of resolving the "Missing Energy Problem" of TDEs (Lu & Kumar, 2018). As discussed above, the efficiency of accretion is very high, and if most of a star is accreted onto a BH, the energy budget is $\sim 10^{52} - 10^{53}$ erg. However, TDEs observed in the UV/optical regime only display radiated energies $\sim 10^{51}$ erg. This implies that the process is either very radiatively inefficient (Curd & Narayan, 2019) or the energy is being emitted at wavelengths we do not observe, such as if the radiation is in the far-UV, or in a relativistic jet that is beamed away from our LoS (see e.g. Lu & Kumar, 2018; Dai et al., 2018; Jonker et al., 2020). If the environment around the AGN is dense, it can reprocess UV and X-rays that would otherwise go unobserved, potentially producing an IR echo, which we can then observe. In this case, the temperature of the echo and the delay time between the UV/optical and IR flare allows a measurement of the peak luminosity of the TDE over the wavelength range of efficient dust absorption (Jiang et al., 2016)

Hills (1975) originally studied the concept of TDEs within the context of stars being the fuel for observed AGN. This naturally provoked the question of TDE rates, or more specifically, how many stars will pass the Roche limit of a SMBH? As described in Stone et al. (2020), in a galactic nuclei without an AGN, the stellar orbits are primarily determined by a combination of the background gravitational potential and discrete scattering events with other stars. These discrete scattering events are the primary cause for stars to be sent into orbits that lead to their tidal disruption. Studies in the 70's showed that TDEs were insufficient to fuel the AGN, except for in cases where the stellar density was so high that other effects (such as stellar collisions) would anyway dominate (Young et al., 1977; Frank & Rees, 1976), but the question of TDE rates retained its interest. The theoretical TDE rate is well-studied both analytically and in numerical simulations and studies of the rate due to two-body scattering between stars is found to be $\sim 10^{-4}$ yr^{-1} galaxy^{-1} (e.g. Wang & Merritt, 2004; Magorrian & Tremaine, 1999). However, a number of effects such as the presence of a binary SMBH system (Milosavljević & Merritt, 2003; Merritt & Milosavljević, 2005) or an AGN accretion disk (Karas & Šubr, 2007) can increase this rate in specific galaxies.

The rate of TDEs inferred from the early X-ray (Donley et al., 2002), UV (Gezari et al., 2008) and optical (van Velzen & Farrar, 2014) observations was $\sim 10^{-5}$ yr^{-1} galaxy^{-1}, an order of magnitude less than the estimates above. However, the low number of events and uncertainty as to the completeness of these surveys made this effect likely to not be physical, and indeed as more TDEs are detected in more complete surveys recent studies find a observed rate of $\sim 10^{-4}$ yr^{-1} galaxy^{-1} (van Velzen, 2018; Hung et al., 2018). These studies also find that a statistically significant association between TDEs and galaxies that have SMBHs less massive than the Hills mass, as predicted from theory (van Velzen, 2018).

Study of the hosts of observed TDEs displayed a surprising preference for post-starburst/E+A galaxies: galaxies that show spectral features that indicate little ongoing star formation but significant star formation in the last ∼Gyr (e.g. Arcavi et al., 2014; French et al., 2016). This feature could indicate a recent galaxy-galaxy merger event (e.g. Yang et al., 2004). These galaxies have a number of features that could lead them to exhibit elevated TDE rates: a potential SMBH binary system, a population of stars on disturbed orbits leading them close to the BH and/or a population of stars that could evolve into giants that are more easily disrupted (see French et al., 2016, 2020, and refs therein).

As this summary has made clear, the study of TDEs is a vibrant and evolving field with still many unanswered questions and ongoing discoveries. I will now describe a subset of these discoveries, TDEs and TDE candidates discovered in the IR.

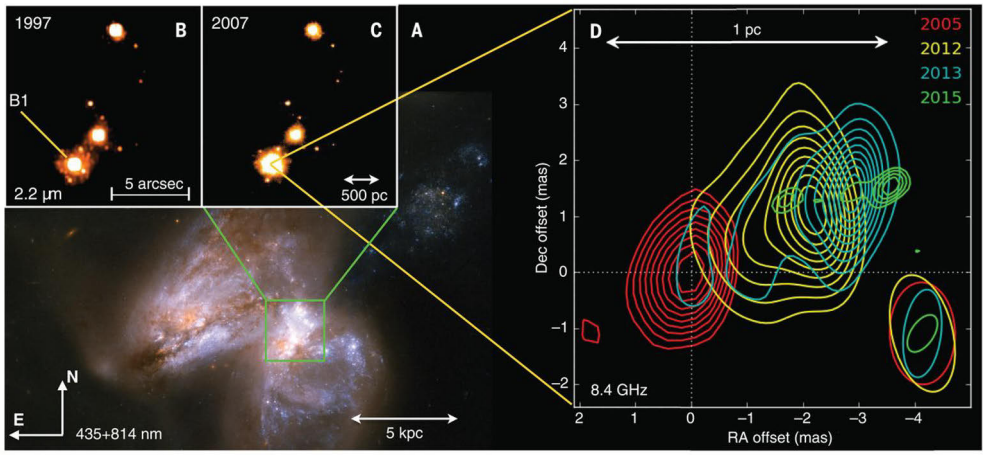

Figure 14. Figure taken from Mattila et al. (2018) that shows Arp 299-B AT1 at multiple physical scales and wavelengths. Section A on the left side of the image shows a colour-composite optical HST image of the entire galaxy Arp 299, with its complicated structure clearly visible. The inset K-band images in the top left show some of the nuclei of the galaxy system, with the B1 nucleus, clearly brightening from the epoch shown in section B to the epoch shown in section C. Section D on the right displays the evolution of the radio data over time, in which an initially unresolved radio source becomes a resolved jet, and the emission moves westward over time. The radio beam size for each epoch is shown in the bottom right.

3.3 Nuclear transients in luminous infrared galaxies

As discussed in Sect. 2.3.3, there are strong incentives to detect and study SNe in LIRGs. However, in the course of observing these galaxies there have been a number of fortuitous discoveries of nuclear transients. These transients present unusual features not consistent with typical AGN activity, and at least one can be firmly identified as a TDE.

3.3.1 Arp 299−B AT1

In Mattila et al. (2018), the authors describe a long lived IR transient in the galaxy Arp 299. This galaxy (shown in Fig. 14) is a LIRG with $\log(L_{IR}/L_{\odot}) \sim 11.9$ and displays a complicated structure indicating a recent ongoing merger. The transient, hereafter referred to as Arp 299−B AT1, is coincident with one of the nuclei (called B1) of the galaxy. The evolution of the transient in IR is slow: it was discovered in 2005 and still has not returned to the pre−explosion level in MIR observations at time of writing. There is little evidence of any optical or UV transient, with only a single faint I-band detection in late-time HST imaging that may be unrelated to the IR/radio transient. There is a concealed AGN within the B1 nucleus, which is seen at an almost edge-on viewing angle (Alonso-Herrero et al., 2013) implying that the central BH is obscured behind a massive dusty torus. This AGN is addition-

ally detected in hard X-rays, with evidence of very strong absorption, supporting the edge-on interpretation (Della Ceca et al., 2002). BB fitting to the slowly evolving IR transient reveals a slow decline in temperature and increase in radius, characteristic of absorption and re-radiation of light from UV and optical emission by dust. Integrating the luminosity of the BB over time yields a lower limit on the total radiated energy of $\sim 1.5 \times 10^{52}$ erg. The most spectacular observations associated with this transient come from the radio. As shown in Fig. 14, a resolved radio source was detected around the time of the transient discovery, that then moved away from the original position over time. This is consistent with the launch of a jet associated with an accretion event onto the central SMBH.

This transient can be best explained by a TDE. The characteristics of the jet implied from the radio observations are consistent with those from TDE models. Crucially, the angle of the jet with respect to the LoS is well constrained to $25°-35°$ by its apparent velocity and the absence of a counter jet. If the jet was produced by enhanced accretion from an existing accretion disk associated with the AGN, the jet would be expected to be close to 90° to the LoS in order to be consistent with the close to edge-on viewing angle for the AGN, while a TDE jet has no such constraint. Fitting the IR SED of the B1 nucleus with radiative transfer models for emission from dust heated by different nuclear sources, both before and after outburst, suggest that the emission observed in the IR can be explained by reprocessing of the TDE light by dust in the polar regions above the AGN, which would be relatively un−obscured by the dusty torus. SED modelling yields a value for the covering factor of the polar dust between $23\%-78\%$, which yields radiated energies for the transient consistent with the disruption of a $1.9-6.5\ M_\odot$ star. Such stars would be able to be disrupted by the $2 \times 10^7\ M_\odot$ SMBH (Ptak et al., 2015) within the B1 nucleus of Arp 299.

3.3.2 IRAS F01004−2237

Another surprising and fortuitous discovery of a transient within a LIRG is described in Tadhunter et al. (2017). The authors observed the nucleus of a ULIRG, IRAS F01004-2237, with optical spectroscopy and were surprised to discover that broad ($\sim$ 5000 km s^{-1}) He I and He II lines had appeared in their spectrum that were not present in spectra taken previously. Searching in archival data, they discovered that the galaxy had undergone an optical outburst approximately 5 years before the detection of the new spectral features. Although there is evidence that the galaxy is a Type 2 AGN (Rodríguez Zaurín et al., 2013; Veilleux et al., 2009), the authors consider the transient activity unusual for an AGN, with the flare large for a radio-quiet AGN and He emission lines unusual for CLAGNs in a high state. These lines are more consistent with a TDE, and the magnitude in V-band is consistent with a TDE also, although the optical flux could have suffered from dust extinction. However, the flare lasts unusually long for a TDE (> 5 years). Dou et al. (2017) report on the

detection of an extremely luminous IR echo associated with this transient and suggest it is due to reprocessing by a thick dusty ring at an intermediate viewing angle for the observer. The scattering of optical light by the same dust could explain the long lasting LC of the transient in the optical.

The nature of this event is further discussed in Trakhtenbrot et al. (2019), in which the authors connect the transient in IRAS F01004−2237 with other nuclear transients, AT 2017bgt and OGLE 17aaj (Gromadzki et al., 2019). All of these transients show a broad emission feature at ∼4860 Å which is attributed to He II and N III transitions associated with the Bowen fluorescence mechanism which was described above in Sect. 3.2, and AT 2017bgt shows the O III feature also associated with this process. These features are not seen in typical AGN, although they have been previously predicted (Netzer et al., 1985), and when interpreted as arising from the BLR of an existing AGN, require intense UV continuum emission from the accretion. Trakhtenbrot et al. (2019) disfavour the TDE interpretation for these transients, or at least TDEs similar to those commonly discovered at UV/optical wavelengths, due to the width of the emission features being far narrower than typical for TDEs, as well as the persistence of these features and the slow evolution of the optical LC. They instead suggest other mechanisms such as a sudden increase in accretion related to a SMBH binary system or interaction between an outflow and the BLR, but note that their nature is uncertain.

This transient continues to evolve and there have been further publications describing its spectral evolution. Tadhunter et al. (2021) show that the strength of forbidden emission lines had increased from 2015 to 2018, while the strength of permitted features declined. They interpreted this as the light from a flare exciting gas in an outflow with a light travel time delay and continue to favour the TDE interpretation. They note that TDEs can produce Bowen fluorescence features (see Sect. 3.2) and that without a TDE, an explanation is required as to how an AGN can produce these Bowen features given that a typical Type 2 AGN or CLAGN does not. A suggested explanation is a case in which a TDE occurs in a nucleus with a pre-existing accretion disk, and the interaction of the TDE material with the disk could lead to a unique transient. Models for these events (Chan et al., 2019) indicate that the accretion disk could be disturbed and experience enhanced accretion while it settles back to its previous state, explaining the long lifetime of the transient. Cannizzaro et al. (2021) followed the entire spectral evolution of the transient since discovery and notes that the evolution of emission features is not characteristic of typical AGN behaviour. The He lines become narrower with time, similar to the behaviour in TDEs, rather than broader over time, as would be the expected behaviour as the central flare declined if the lines arose from the BLR of an AGN (see e.g. Peterson et al., 2004). They additionally cast doubt on the Bowen fluorescence features observed in IRAS F01004−2237, noting that the N III features do not increase during the flare, unlike the He II lines, and could arise from the known population of Wolf-Rayet stars in

this galaxy.

3.3.3 Tidal disruption event rates in LIRGs

A striking feature of the discoveries described above is their fortuitous nature, with both Arp 299-B AT1 and the transient in IRAS F01004-2237 arising from observations that were not specifically aiming to detect TDEs. To these we can add a third nuclear transient, AT 2017gbl, which was discovered in the LIRG IRAS 23436+2527 and is described in Paper IV. The transient is similar to the two described above, in that it can be well explained by a TDE, and it was discovered fortuitously as part of a survey searching for SNe. In that survey, multiple LIRGs were monitored and so in Paper IV we derived the rate of AT 2017gbl−like events in LIRGs as 10^n LIRG^{-1} year^{-1} with n $= -1.9^{+0.5}_{-0.8}$, with 1σ uncertainties. Tadhunter et al. (2017) find a similar result of 10^{-2} events year^{-1} LIRG^{-1} inferred from their discovery of the transient in IRAS F01004-2237. This is much higher than the typical rate expected for TDEs, estimated from either observations or theory, of $\sim$10^{-4} year^{-1}. However, this is not inconsistent with expectations: many LIRGs, including Arp 299 and IRAS 23436+5257, are merging systems and, as discussed in Sect. 3.2 in the context of the E+A hosts of UV/optically discovered TDEs, mergers are predicted to have an elevated TDE rate (see e.g. Li et al., 2019). Additionally the presence of multiple SMBHs that could interact in a binary (e.g. Li et al., 2019), high central stellar densities due to the recent starburst (e.g. Pfister et al., 2019) and other more complicated effects (see e.g. Stone et al., 2020, for details) could elevate the TDE rate.

As discussed in Sect. 2.3.3, the dusty environment of LIRGs obscures transients in the optical, which could lead to many TDEs or other nuclear transients within them to be missed by optical surveys, and this effect is exacerbated by the potential obscuration by a dusty AGN torus inferred in the case of Arp 299−B AT1 and AT 2017gbl. Furthermore, even when these transients are detectable in optical surveys, they have likely been previously missed due to their identification as “normal” AGN activity. Paper V describes a search for nuclear transients in LIRGs making use of IR observations in order to detect IR echos and not be affected by obscuration, and improve the rate estimates for such transients in LIRGs.

4 Summary of the articles

In the sections below I briefly describe the content of the articles included in this thesis and their main methods, analysis and results. There are two major research areas covered in the articles. The first is the study of CCSNe and their progenitors, which is the topic of Paper I, Paper II and Paper III. Paper I and Paper III focus on obscured or otherwise difficult to observe CC events, failed CCSN in the case of Paper I and SN hidden in dusty LIRGs in the case of Paper III. Paper II is a case study of a particular luminous Type IIL SN and explores potential scenarios for explaining its characteristics. The second topic is the study of nuclear transients in LIRGs. Paper IV considers a particular nuclear transient discovered in a LIRG and attempts to ascertain the physical nature of the event that caused it. Paper V performs an archival survey to attempt to discover more nuclear transients in LIRGs and investigate the rate that they are occurring. At the end of each of the below sections I summarise my personal contributions to the paper in question.

4.1 Paper I

In Paper I we presented a search for vanishing massive stars in archival HST data, in order to infer the existence of a failed SN. To construct our sample, we began with all galaxies within 28 Mpc, chosen in order to be able to detect and resolve individual massive stars. We then searched the HST archive for galaxies within this sample that had been observed at 3 separate epochs, with the F814W filter (7000-9700Å) and one of the 3 most recent wide-field optical cameras equipped on HST. The red F814W filter allowed us to most efficiently detect the cool RSGs that we expected to vanish. The 3 epoch condition allowed us to reject variables by establishing the source is not variable before it vanishes. We adopted some other minor cuts to the sample, that are described in the article, which left us finally with a sample of 15 galaxies.

In order to detect vanishing stars, we aligned the individual images obtained from the Hubble legacy archive to a common pixel scale and made use of optimal image subtraction which convolves one of the images with a kernel in order to match the point spread function between the images. After subtraction, we identified sources remaining in the image and eyeballed them in order to remove contaminants introduced in the subtraction process. We then searched for sources that were present in both the subtractions involving the 3rd epoch of imaging, indicating a source present

in the first 2 images but not the last. Finally, we performed photometry for the sources detected.

6 candidates were discovered through this process. 2 candidates were identified as variable sources. 3 candidates were found in a particular galaxy system, which consists of a superimposed pair of galaxies which are not physically close. There is therefore doubt about whether these sources are associated with the further or closer galaxy, and they are only consistent with RSGs when associated with the further galaxy. The final source is the best candidate for a failed SN. The pre-disappearance photometry is consistent with a 30 $M_{\odot}$ yellow supergiant star. We consider potential contaminants such as Mira variable stars and reject them for any of our objects. Our detection of 1 candidate is broadly consistent with expectations for the rate of failed SNe obtained by (Neustadt et al., 2021), as 2 CCSNe exploded in our galaxy sample during the survey time.

I performed the entirety of the search section of the project, creating the sample, obtaining the data, performing the alignments and image subtractions, and searching for sources in the subtracted images. I contributed significantly to the preparation of the manuscript, in particular the methods section, and as the corresponding author for the article, led the revision process. As the first author, I contributed the majority of the material in the paper.

4.2 Paper II

In Paper II we presented the follow-up observations of an individual Type IIL SN 2016gsd. This SN was discovered by an amateur astronomer and classified as a Type II SN from a spectrum which showed weak H emission features on a blue continuum. The bright absolute magnitude for a Type II, $M_V \sim -20$ mag, motivated an extensive follow-up campaign consisting of optical and NIR imaging and spectroscopy spanning almost a year. These data was gathered as part of both the Nordic Optical Telescope Unbiased Transient Survey (NUTS[1]) and the extended Public ESO Spectroscopic Survey for Transient Objects (ePESSTO[2]) programmes, both of which I am a member.

The evolution of the LCs of the SN were extremely linear in magnitude across observing bands spanning the entire optical wavelength region. Along with the bright absolute magnitude, this revealed SN 2016gsd as a member of a small group of SNe that have bright peak magnitudes and linear LCs, which includes SN 1979C, SN 1998S and SN 2013fc. The spectra of SN 2016gsd were blue and featureless for $\sim$ 20 days after explosion, before developing broad emission lines of the H Balmer series that exhibit high and persistent velocities for a Type II SNe of $>$15000 km

[1] https://nuts.sn.ie/

[2] https://www.pessto.org/

s^{-1}, measured from the absorption in the P-Cygni profile. Additionally, the metal lines present in the spectra were weak, perhaps indicating a low metallicity for the progenitor star. This is supported by the host galaxy of the SN being a low luminosity dwarf, which typically have low metallicities.

In order to ascertain the likely characteristics of the progenitor of this SN, we attempted to model its LC and spectra with the spectral synthesis code JEKYLL (Ergon et al., 2018). We constructed a progenitor with an extended low mass envelope in order to attempt to produce the large peak luminosity and fast decline of the LCs, but found that this model was insufficient to reproduce all of the observed characteristics. Our favoured explanation for this is the presence of CSM interaction, evidence for which is seen in our data in the form of the long lasting early blue continuum phase, intermediate width spectral features, and a late time H alpha emission feature. The presence of CSM can also help produce the bright peak magnitude of the SN and mask the expected drop in the LC at the photospheric - nebular transition, which is not clear in our observations. CSM interaction is clearly detected in other SNe with similar characteristics such as SN 1979C and SN 1998S.

However, tensions with the CSM power interpretation arise in the form of the high velocities seen even at late times, and strong H absorption feature. The late time velocities should be suppressed if the kinetic energy of the explosion is converted into radiated energy through collision with slow moving CSM, and the presence of very fast moving H at late times implies a direction along which the material can escape without strong interaction with CSM. Finally, our spectrum at late times shows weak or no nebular features associated with [O I], indicating that the progenitor star was likely not more massive than 15 $M_{\odot}$. In order to produce a dense enough asymmetrical CSM from a low-metallicity star of this mass, a binary scenario may need to be invoked.

I organised the follow-up campaign of SN 2016gsd and arranged the majority of the data collection. I reduced some of the photometric and about half of the spectroscopic data and performed close to all of the analysis, outside of the modelling. I wrote the large majority of the text in the manuscript. I was the first author and I contributed a large majority of the material of the paper.

4.3 Paper III

In Paper III we presented the SUNBIRD (Supernova UNmasked By Infrared Detection) project, a search for SNe in LIRGs making use of laser guide star adaptive optics (LGSAO) NIR observations. SNe in LIRGs often suffer from large extinction due to their dusty LIRG environment, necessitating observations in the IR where the effect of extinction is much less. The AO system enables observations with a spatial resolution of $\sim$0.1 arcsecond, allowing us to resolve transients in the complicated background very close to the nuclei of galaxies, which had proven previously to be

effective at finding SNe in LIRGs (Mattila et al., 2007; Kankare et al., 2008, 2012).

4 SNe were discovered, and these were identified as CCSNe through fitting to template LCs, where the multi-band JHK data are simultaneously fit to well observed SNe LCs with the extinction, explosion date and a constant shift in magnitude as free parameters. This is necessary for classification, as spectroscopy is often difficult to obtain for these objects, due to their optical faintness and the frequently long time delay between the explosion and discovery. The SNe were classified as likely Type II, or Type IIP SNe, with extinctions varying between 0 and 5 magnitudes in V-band. 2 of the SN were located within 1 kpc of the galaxy nucleus and, considering the entire sample of SN discovered in LIRGs, we show that NIR AO is much more effective than both optical and non-AO NIR searches at finding SNe close to galaxy nuclei. We consider the detection efficiency of the survey through simulation of artificial sources in the images followed by recovery after subtraction, and show that detection in the very central 100 pc of the galaxy remains very difficult.

I provided the detection efficiency estimates for this survey and wrote that section of the manuscript. I reduced and performed subtractions for the data taken with the VLT NACO instrument and obtained and reduced data taken with the NOTCam and ALFOSC instruments on the Nordic Optical Telescope. I was involved in discussion about the project throughout its progress and helped to prepare the manuscript. As a co-author I contributed a minority of the material in the paper.

4.4 Paper IV

In Paper IV we described the discovery, follow-up, analysis and interpretation of a nuclear transient discovered during the SUNBIRD survey. The transient was discovered in LGSAO imaging with the KECK telescope, coincident with the northern nucleus of the LIRG IRAS 23436+5257. NIR and optical imaging follow-up, along with observations from the Wide-field Infrared Survey Explorer (WISE) in the MIR, revealed a bright IR transient that evolved slowly over $\sim$ 2 years along with a faint and rapidly declining optical outburst. We additionally obtained spectroscopy both in the IR and optical, as well as radio and X-ray follow-up. Much of the optical and NIR follow-up was obtained from the aforementioned NUTS collaboration.

The IR data was well-fit with a BB, declining in temperature over time, implying an IR echo from dust heated by an outburst associated with the SMBH in the galaxy nucleus. Broad ($\sim$2000 km s^{-1}) emission lines of H, He I and O I were observed in spectra taken shortly after the flare, and then declined over time. SED fitting of the galaxy indicated the presence of a Type 2 AGN, consistent with the slow MIR variability observed before the outburst. This meant that the central engine of the AGN is likely obscured by the dusty torus. However, measurement of H emission lines yield an estimate of only 2.5 magnitudes of extinction in V-band. We argue this could be explained by the lines being scattered from the polar regions above the

AGN. Fitting the optical and IR photometry with two BBs, one obscured by these 2.5 magnitudes of extinction, yields a hot BB of ~ 6500 K.

We favour the explanation of a SMBH related transient for AT 2017gbl, as its total radiated energy, radio evolution and IR luminosity are inconsistent with those of a SN. The full−width half maxima of the measured broad lines are consistent with the broad lines present in Type 1 AGN. We interpret these lines as originating in the BLR of the AGN, having been illuminated by an accretion event, and then scattered from the polar region into our LoS. The fast rise of the IR echo from AT 2017gbl, $<$140 days, contrasts it with other nuclear transients in LIRGs such as Arp 299−B AT1 (Mattila et al., 2018) and IRAS F01004-2237 (Dou et al., 2017) and additionally is unlike any previously observed CLAGN. AT 2017gbl shows radio variability, unlike almost all CLAGNs recorded. Given these features, we consider that AT 2017gbl could also have been powered by a TDE. We calculated the SMBH mass in this nucleus of IRAS 23436+5257 as $\log_{10}(M_{BH}/M_{\odot}) = 7.1 \pm 0.4$, which is sufficiently low mass to disrupt a star. The IR echo and optical evolution were consistent in terms of timescale with other TDEs, although the echo was much more luminous. The lack of typical TDE features in the spectra would be due to the obscuration of the TDE accretion disk by the dusty torus.

For this project, I obtained and reduced the optical and NIR imaging and some of the optical spectra. I performed all analysis related to the optical and NIR spectroscopy. I wrote all sections of the manuscript related to the spectroscopy. I worked closely with the first author at all stages of the project, and contributed heavily to most other sections of the manuscript. As 2nd author, I made the 2nd largest contribution to the paper.

4.5 Paper V

In Paper V we described an archival survey in which we search for nuclear transients in LIRGs making use of the MIR observations taken by the WISE satellite. The NEOWISE survey makes uses of the WISE satellite to observe the entire sky every 6 months at 3.4 and 4.6μm, and is effective in detecting IR echos in galaxy nuclei, such as those discussed in Sect. 3.3. We took the sample of LIRGs from the Revised Bright Galaxy Sample (RBGS) (Sanders et al., 2003) and processed the NEOWISE data for these objects. We searched for luminous outbursts in galaxies that do not show clear signs of stochastic variability in their MIR LCs.

We discovered 5 objects in our sample, 2 of which are the previously published transients Arp 299-B AT1 (Mattila et al., 2018) and AT 2017gbl (Paper IV). We investigate the available archive data to search for any optical outbursts associated with the IR transients, finding none. We fit BBs to the MIR data to investigate the properties of the dust echo, and show that this method applied to only 2 data points is consistent to previous BB fits in the literature with more data. We consider the

host galaxies of the transients and fit their SEDs, finding strong AGN components in the hosts of the newly discovered transients. We discuss the interpretation of these objects, comparing to previously known transients in the literature, and discuss whether they can be interpreted as TDEs. Based on these discoveries, we evaluate the rate of such transients in LIRGs.

I obtained, processed and analysed all the data considered in the paper, either from public archives or as part of follow-up campaigns. I performed all the analysis in the paper, except for the SED fitting of host galaxies. I wrote the majority of the manuscript, and as first author contributed the large majority of the material in the paper.

5 Future Work

Although the era of all-sky high cadence surveys has already arrived, yielding vast quantities of transient discoveries, new surveys are soon to begin that will push the volume of discovered transients to new heights. The 10-year Legacy Survey of Space and Time (LSST) based at the Rubin observatory will make use of a 8.4 m telescope with an exceptionally wide field of view and a depth much greater than previous surveys and is due to be begun in 2023. It will detect bright events out to great distances, for example detecting 40% of all Type Ia SNe out to a redshift of 0.5 (LSST Science Collaboration et al., 2017). Additionally, such surveys have potential in detecting faint transients, such as those associated with failed SNe. However, filtering for the most interesting objects in the torrent of detected transients in order to trigger follow-up observations and the spectroscopy that is vital for understanding their nature will be a great challenge for astronomers in the next decade.

Even new optical surveys which can observe to greater depths will continue to struggle to detect transients that are heavily extincted in the optical, particularly in complicated nuclear regions of LIRGs. The Nancy Grace Roman Space Telescope, (Roman Telescope), previously known as the Wide-Field IR Survey Telecope (WFIRST) (Akeson et al., 2019), with aimed launch date in 2025, presents a better option for detecting these objects, as it aims to perform an IR imaging survey with both the high resolution available to space based observations and a five day cadence facilitated by its wide field of view. Meanwhile, the NEOWISE survey is continuing to at least 2023, and will provide opportunities to detect and observe the dust echoes of many more TDEs. The James Webb Space Telescope (JWST) is planned to be launched this year, and has the capability to observe the spectroscopic evolution of IR echoes, mapping out the dust present in the interior of an AGN at distance scales that are impossible to resolve for all but the most nearby galaxies.

I plan to continue to work on the IR nuclear transients presented in Paper V. Our understanding of the individual transients can be furthered by performing more complicated modelling of the IR echoes that occur, which requires multi-wavelength data in order to constrain various parameters. Continued discovery and follow-up of these objects is required to provide these data. Investigation of SNe such as SN 2016gsd will continue, with the new surveys mentioned above able to identify SNe with similar properties more rapidly and trigger earlier follow-up. New instruments such as the Son of X-Shooter (SoXS) which will be mounted on the European Southern Ob-

servatory New Technology Telescope, and the NOT Transient Explorer (NTE), to be mounted on the Nordic Optical Telescope, will replace the spectrographs that I made use of to study SN 2016gsd, and provide a huge increase in resolving power as well as simultaneous optical and NIR coverage in the same exposure. Early detection and improved instruments will enable the study of narrow lines at early times that is crucial to understand the CSM interaction present in these SNe.

The search for failed SNe continues with the "survey about nothing" team continuing to observe and improve their statistics, while new HST observations expand the sample size of useful data in the HST archive for finding vanishing stars. Finally, the detection efficiency methodology described in Sect. 4.3 can be expanded to the whole dataset of AO observations of LIRGs, accumulated by the SUNBIRD and previous surveys, which consists of hundreds of images across approximately a decade of observing, in order to establish the best estimate of the intrinsic SN rates in LIRGs. The Extremely Large Telescope's Multi-AO Imaging Camera for Deep Observations (MICADO) instrument represents the next generation of facilities for studying the obscured inner regions of LIRGs and perhaps finally unveiling SNe occurring within the central few tens of parsecs of the nucleus.

List of References

Abbott B. P., et al., 2009, Reports on Progress in Physics, 72, 076901
Abbott B. P., et al., 2016, Phys. Rev. Lett, 116, 241103
Abramovici A., et al., 1992, Science, 256, 325
Adams S. M., Kochanek C. S., Gerke J. R., Stanek K. Z., Dai X., 2017a, MNRAS, 468, 4968
Adams S. M., Kochanek C. S., Gerke J. R., Stanek K. Z., 2017b, MNRAS, 469, 1445
Akeson R., et al., 2019, arXiv e-prints, p. arXiv:1902.05569
Alexander K. D., Berger E., Guillochon J., Zauderer B. A., Williams P. K. G., 2016, ApJl, 819, L25
Alexander K. D., van Velzen S., Horesh A., Zauderer B. A., 2020, Space Sci. Rev., 216, 81
Alonso-Herrero A., et al., 2013, ApJl, 779, L14
Anderson J. P., et al., 2014a, MNRAS, 441, 671
Anderson J. P., et al., 2014b, ApJ, 786, 67
Anderson J. P., et al., 2018, Nature Astronomy, 2, 574
Antonucci R., 1993, ARA&A, 31, 473
Antonucci R. R. J., Miller J. S., 1985, ApJ, 297, 621
Arcavi I., et al., 2012, ApJl, 756, L30
Arcavi I., et al., 2014, ApJ, 793, 38
Aretxaga I., Benetti S., Terlevich R. J., Fabian A. C., Cappellaro E., Turatto M., della Valle M., 1999a, MNRAS, 309, 343
Aretxaga I., Joguet B., Kunth D., Melnick J., Terlevich R. J., 1999b, ApJl, 519, L123
Arnett D., 1996, Supernovae and Nucleosynthesis: An Investigation of the History of Matter from the Big Bang to the Present
Baade W., 1945, ApJ, 102, 309
Baade W., Zwicky F., 1934a, Proceedings of the National Academy of Science, 20, 254
Baade W., Zwicky F., 1934b, Proceedings of the National Academy of Science, 20, 259
Bade N., Komossa S., Dahlem M., 1996, A&A, 309, L35
Barbon R., Ciatti F., Rosino L., 1979, A&A, 72, 287
Barbon R., Ciatti F., Rosino L., 1982, A&A, 116, 35
Barvainis R., 1987, ApJ, 320, 537
Basinger C. M., Kochanek C. S., Adams S. M., Dai X., Stanek K. Z., 2020, arXiv e-prints, p. arXiv:2007.15658
Beals C. S., 1929, MNRAS, 90, 202
Beasor E. R., Davies B., Smith N., van Loon J. T., Gehrz R. D., Figer D. F., 2020, MNRAS, 492, 5994
Bethe H. A., 1990, Reviews of Modern Physics, 62, 801
Blagorodnova N., et al., 2019, ApJ, 873, 92
Blanchard P. K., et al., 2017, ApJ, 843, 106
Blandford R., Meier D., Readhead A., 2019, ARA&A, 57, 467
Blinnikov S. I., Bartunov O. S., 1993, A&A, 273, 106
Blondin J. M., Mezzacappa A., DeMarino C., 2003, ApJ, 584, 971
Boller T., Brandt W. N., Fink H., 1996, A&A, 305, 53
Bondi M., Pérez-Torres M. A., Herrero-Illana R., Alberdi A., 2012, A&A, 539, A134
Bonnerot C., Rossi E. M., Lodato G., 2017, MNRAS, 464, 2816
Borst L. B., 1950, Physical Review, 78, 807

Bostroem K. A., et al., 2019, MNRAS, 485, 5120
Botticella M. T., Smartt S. J., Kennicutt R. C., Cappellaro E., Sereno M., Lee J. C., 2012, A&A, 537, A132
Bowen I. S., 1934, PASP, 46, 146
Branch D., Falk S. W., McCall M. L., Rybski P., Uomoto A. K., Wills B. J., 1981, ApJ, 244, 780
Braun H., Langer N., 1995, A&A, 297, 483
Burrows A., Lattimer J. M., 1986, ApJ, 307, 178
Cannizzaro G., Jonker P. G., Mata-Sánchez D., 2021, ApJ, 909, 159
Cao Y., et al., 2013, ApJl, 775, L7
Cappellaro E., et al., 2015, A&A, 584, A62
Caprioli D., Spitkovsky A., 2014a, ApJ, 783, 91
Caprioli D., Spitkovsky A., 2014b, ApJ, 794, 46
Caprioli D., Spitkovsky A., 2014c, ApJ, 794, 47
Carter B., Luminet J. P., 1983, A&A, 121, 97
Castor J. I., Lamers H. J. G. L. M., 1979, ApJs, 39, 481
Castor J. I., Abbott D. C., Klein R. I., 1975, ApJ, 195, 157
Chan C.-H., Piran T., Krolik J. H., Saban D., 2019, ApJ, 881, 113
Chevalier R. A., 1982, ApJ, 259, 302
Chevalier R. A., Fransson C., 1994, ApJ, 420, 268
Chevalier R. A., Fransson C., 2001, ApJl, 558, L27
Chevalier R. A., Fransson C., Nymark T. K., 2006, ApJ, 641, 1029
Chiosi C., Maeder A., 1986, ARA&A, 24, 329
Chomiuk L., Povich M. S., 2011, AJ, 142, 197
Chugai N. N., 2001, MNRAS, 326, 1448
Chugai N. N., et al., 2004, MNRAS, 352, 1213
Clavel J., Wamsteker W., Glass I. S., 1989, ApJ, 337, 236
Colgate S. A., Johnson M. H., 1960, Phys. Rev. Lett, 5, 235
Colgate S. A., McKee C., 1969, ApJ, 157, 623
Curd B., Narayan R., 2019, MNRAS, 483, 565
Dahlen T., Strolger L.-G., Riess A. G., Mattila S., Kankare E., Mobasher B., 2012, ApJ, 757, 70
Dai L., McKinney J. C., Roth N., Ramirez-Ruiz E., Miller M. C., 2018, ApJl, 859, L20
Davies B., Beasor E. R., 2018, MNRAS, 474, 2116
Davies B., Beasor E. R., 2020, MNRAS, 496, L142
Della Ceca R., et al., 2002, ApJl, 581, L9
Dessart L., Hillier D. J., 2005, A&A, 437, 667
Dessart L., Hillier D. J., Audit E., Livne E., Waldman R., 2016, MNRAS, 458, 2094
Dexter J., Agol E., 2011, ApJl, 727, L24
Doggett J. B., Branch D., 1985, AJ, 90, 2303
Donley J. L., Brandt W. N., Eracleous M., Boller T., 2002, AJ, 124, 1308
Dou L., Wang T., Yan L., Jiang N., Yang C., Cutri R. M., Mainzer A., Peng B., 2017, ApJl, 841, L8
Dwek E., 1983, ApJ, 274, 175
Ekström S., et al., 2012, A&A, 537, A146
Elias-Rosa N., et al., 2011, ApJ, 742, 6
Elias J. H., Matthews K., Neugebauer G., Persson S. E., 1985, ApJ, 296, 379
Ergon M., et al., 2015, A&A, 580, A142
Ergon M., Fransson C., Jerkstrand A., Kozma C., Kromer M., Spricer K., 2018, A&A, 620, A156
Ertl T., Janka H. T., Woosley S. E., Sukhbold T., Ugliano M., 2016, ApJ, 818, 124
Evans C. R., Kochanek C. S., 1989, ApJl, 346, L13
Faran T., et al., 2014, MNRAS, 445, 554
Fassia A., et al., 2000, MNRAS, 318, 1093
Fassia A., et al., 2001, MNRAS, 325, 907
Feldmeier A., 1995, A&A, 299, 523

Filippenko A. V., 1997, ARA&A, 35, 309
Filippenko A. V., Matheson T., Ho L. C., 1993, ApJl, 415, L103
Filippenko A. V., et al., 1995, ApJl, 450, L11
Folatelli G., et al., 2016, ApJl, 825, L22
Fox O. D., et al., 2014, ApJ, 790, 17
Fox O. D., et al., 2021, MNRAS,
Frank J., Rees M. J., 1976, MNRAS, 176, 633
Frank J., King A., Raine D. J., 2002, Accretion Power in Astrophysics: Third Edition
Fransson C., 1982, A&A, 111, 140
Fransson C., et al., 2014, ApJ, 797, 118
Frederick S., et al., 2020, arXiv e-prints, p. arXiv:2010.08554
French K. D., Arcavi I., Zabludoff A., 2016, ApJl, 818, L21
French K. D., Wevers T., Law-Smith J., Graur O., Zabludoff A. I., 2020, Space Sci. Rev., 216, 32
Fryer C. L., 1999, ApJ, 522, 413
Gafton E., Rosswog S., 2019, MNRAS, 487, 4790
Gal-Yam A., 2017, Observational and Physical Classification of Supernovae. p. 195, doi:10.1007/978-3-319-21846-5_35
Gal-Yam A., Leonard D. C., 2009, Nature, 458, 865
Gal-Yam A., et al., 2014, Nature, 509, 471
Galama T. J., et al., 1999, A&As, 138, 465
Galbany L., et al., 2016, AJ, 151, 33
Garnavich P. M., Tucker B. E., Rest A., Shaya E. J., Olling R. P., Kasen D., Villar A., 2016, ApJ, 820, 23
Gerke J. R., Kochanek C. S., Stanek K. Z., 2015, MNRAS, 450, 3289
Gezari S., 2021, arXiv e-prints, p. arXiv:2104.14580
Gezari S., et al., 2006, ApJl, 653, L25
Gezari S., et al., 2008, ApJ, 676, 944
Gezari S., et al., 2009a, ApJ, 690, 1313
Gezari S., et al., 2009b, ApJ, 698, 1367
Gezari S., et al., 2010, ApJl, 720, L77
Gezari S., et al., 2012, Nature, 485, 217
Gezari S., et al., 2015, ApJ, 804, 28
Goodrich R. W., 1989a, ApJ, 340, 190
Goodrich R. W., 1989b, ApJ, 342, 224
Graham J. R., et al., 1983, Nature, 304, 709
Graham M. J., Djorgovski S. G., Drake A. J., Stern D., Mahabal A. A., Glikman E., Larson S., Christensen E., 2017, MNRAS, 470, 4112
Grassberg E. K., Imshennik V. S., Nadyozhin D. K., 1971, Ap&SS, 10, 28
Greiner J., Schwarz R., Zharikov S., Orio M., 2000, A&A, 362, L25
Gromadzki M., et al., 2019, A&A, 622, L2
Gröningsson P., et al., 2008, A&A, 479, 761
Grupe D., Thomas H. C., Leighly K. M., 1999, A&A, 350, L31
Guhathakurta P., Draine B. T., 1989, ApJ, 345, 230
Guillochon J., Ramirez-Ruiz E., 2013, ApJ, 767, 25
Guillochon J., Ramirez-Ruiz E., 2015, ApJ, 809, 166
Guillochon J., Manukian H., Ramirez-Ruiz E., 2014, ApJ, 783, 23
Hanke F., Marek A., Müller B., Janka H.-T., 2012, ApJ, 755, 138
Heger A., Woosley S. E., 2002, ApJ, 567, 532
Hellings P., 1983, Ap&SS, 96, 37
Hellings P., 1984, Ap&SS, 104, 83
Hernández-García L., Masegosa J., González-Martín O., Márquez I., Guainazzi M., Panessa F., 2017, A&A, 602, A65

Hillier D. J., Dessart L., 2019, A&A, 631, A8
Hills J. G., 1975, Nature, 254, 295
Holoien T. W. S., et al., 2020, ApJ, 898, 161
Horiuchi S., Beacom J. F., Kochanek C. S., Prieto J. L., Stanek K. Z., Thompson T. A., 2011, ApJ, 738, 154
Houck J. R., Schneider D. P., Danielson G. E., Beichman C. A., Lonsdale C. J., Neugebauer G., Soifer B. T., 1985, ApJl, 290, L5
Humphreys R. M., Davidson K., 1994, PASP, 106, 1025
Humphreys R. M., et al., 1997, AJ, 114, 2778
Hung T., et al., 2018, ApJs, 238, 15
Hung T., et al., 2019, ApJ, 879, 119
Iwamoto K., et al., 2000, ApJ, 534, 660
Janka H.-T., 2012, Annual Review of Nuclear and Particle Science, 62, 407
Janka H. T., Langanke K., Marek A., Martínez-Pinedo G., Müller B., 2007, Phys. Rep., 442, 38
Janka H.-T., Melson T., Summa A., 2016, Annual Review of Nuclear and Particle Science, 66, 341
Jencson J. E., et al., 2019, ApJ, 886, 40
Jerkstrand A., Smartt S. J., Fraser M., Fransson C., Sollerman J., Taddia F., Kotak R., 2014, MNRAS, 439, 3694
Jiang N., Dou L., Wang T., Yang C., Lyu J., Zhou H., 2016, ApJl, 828, L14
Jonker P. G., et al., 2013, ApJ, 779, 14
Jonker P. G., Stone N. C., Generozov A., van Velzen S., Metzger B., 2020, ApJ, 889, 166
Kangas T., Mattila S., Kankare E., Kotilainen J. K., Väisänen P., Greimel R., Takalo A., 2013, MNRAS, 436, 3464
Kankare E., et al., 2008, ApJl, 689, L97
Kankare E., et al., 2012, ApJl, 744, L19
Kankare E., et al., 2014, MNRAS, 440, 1052
Kankare E., et al., 2017, Nature Astronomy, 1, 865
Kankare E., et al., 2021, A&A, 649, A134
Karas V., Šubr L., 2007, A&A, 470, 11
Kasen D., Woosley S. E., 2009, ApJ, 703, 2205
Kelly B. C., Bechtold J., Siemiginowska A., 2009, ApJ, 698, 895
Kennicutt Robert C. J., 1998, ARA&A, 36, 189
Kerr R. P., 1963, Phys. Rev. Lett, 11, 237
Kesden M., 2012, Phys. Rev. D, 85, 024037
Khachikian E. Y., Weedman D. W., 1971, ApJl, 164, L109
Khazov D., et al., 2016, ApJ, 818, 3
Kilpatrick C. D., et al., 2021, MNRAS, 504, 2073
Kippenhahn R., Weigert A., Weiss A., 2012, Stellar Structure and Evolution, doi:10.1007/978-3-642-30304-3.
Kochanek C. S., Beacom J. F., Kistler M. D., Prieto J. L., Stanek K. Z., Thompson T. A., Yüksel H., 2008, ApJ, 684, 1336
Kokubo M., 2015, MNRAS, 449, 94
Komossa S., Greiner J., 1999, A&A, 349, L45
Kool E. C., et al., 2018, MNRAS, 473, 5641
Kool E. C., et al., 2020, MNRAS, 498, 2167
Koshida S., et al., 2009, ApJl, 700, L109
Koshida S., et al., 2014, ApJ, 788, 159
Kozłowski S., et al., 2010, ApJ, 708, 927
Kozłowski S., Kochanek C. S., Ashby M. L. N., Assef R. J., Brodwin M., Eisenhardt P. R., Jannuzi B. T., Stern D., 2016, ApJ, 817, 119
Krolik J., Piran T., Svirski G., Cheng R. M., 2016, ApJ, 827, 127
Kroupa P., 2002, Science, 295, 82

LSST Science Collaboration et al., 2017, arXiv e-prints, p. arXiv:1708.04058
LaMassa S. M., et al., 2015, ApJ, 800, 144
Lacy J. H., Townes C. H., Hollenbach D. J., 1982, ApJ, 262, 120
Langer N., 2012, ARA&A, 50, 107
Langer N., et al., 2020, A&A, 638, A39
Lawrence A., et al., 2016, MNRAS, 463, 296
Leloudas G., et al., 2019, ApJ, 887, 218
Leonard D. C., Filippenko A. V., Barth A. J., Matheson T., 2000, ApJ, 536, 239
Leonard D. C., et al., 2002, PASP, 114, 35
Levinson A., Nakar E., 2020, Phys. Rep., 866, 1
Li W., et al., 2011, MNRAS, 412, 1441
Li S., Berczik P., Chen X., Liu F. K., Spurzem R., Qiu Y., 2019, ApJ, 883, 132
Limongi M., Chieffi A., 2006, ApJ, 647, 483
Lin D., et al., 2017, Nature Astronomy, 1, 0033
Lira P., Arévalo P., Uttley P., McHardy I., Breedt E., 2011, MNRAS, 415, 1290
Lodato G., Rossi E. M., 2011, MNRAS, 410, 359
Lodato G., King A. R., Pringle J. E., 2009, MNRAS, 392, 332
Lovegrove E., Woosley S. E., 2013, ApJ, 769, 109
Lu W., Kumar P., 2018, ApJ, 865, 128
Lu W., Kumar P., Evans N. J., 2016, MNRAS, 458, 575
Lucy L. B., Solomon P. M., 1970, ApJ, 159, 879
Lundqvist P., Fransson C., 1988, A&A, 192, 221
MacFadyen A. I., Woosley S. E., Heger A., 2001, ApJ, 550, 410
MacLeod C. L., et al., 2012, ApJ, 753, 106
MacLeod C. L., et al., 2016, MNRAS, 457, 389
Madau P., Dickinson M., 2014, ARA&A, 52, 415
Magnelli B., Elbaz D., Chary R. R., Dickinson M., Le Borgne D., Frayer D. T., Willmer C. N. A., 2009, A&A, 496, 57
Magnelli B., Elbaz D., Chary R. R., Dickinson M., Le Borgne D., Frayer D. T., Willmer C. N. A., 2011, A&A, 528, A35
Magorrian J., Tremaine S., 1999, MNRAS, 309, 447
Maguire K., et al., 2010, MNRAS, 404, 981
Maiolino R., Vanzi L., Mannucci F., Cresci G., Ghinassi F., Della Valle M., 2002, A&A, 389, 84
Mannucci F., et al., 2003, A&A, 401, 519
Mannucci F., Della Valle M., Panagia N., 2007, MNRAS, 377, 1229
Margalit B., Metzger B. D., 2017, ApJl, 850, L19
Mason B. D., Hartkopf W. I., Gies D. R., Henry T. J., Helsel J. W., 2009, AJ, 137, 3358
Mattila S., Meikle W. P. S., 2001, MNRAS, 324, 325
Mattila S., et al., 2007, ApJl, 659, L9
Mattila S., et al., 2012, ApJ, 756, 111
Mattila S., et al., 2018, Science, 361, 482
Maund J. R., Smartt S. J., Kudritzki R. P., Podsiadlowski P., Gilmore G. F., 2004, Nature, 427, 129
Maund J. R., Fraser M., Reilly E., Ergon M., Mattila S., 2015, MNRAS, 447, 3207
Maury A. C., Pickering E. C., 1897, Annals of Harvard College Observatory, 28, 1
McCray R., Fransson C., 2016, ARA&A, 54, 19
McCrea W. H., 1929, Zeitschrift fur Physik, 57, 367
Merritt D., Milosavljević M., 2005, Living Reviews in Relativity, 8, 8
Metzger B. D., Stone N. C., 2017, ApJ, 844, 75
Meynet G., et al., 2015, A&A, 575, A60
Miller M. C., 2015, ApJ, 805, 83
Miller C. J., Nichol R. C., Gómez P. L., Hopkins A. M., Bernardi M., 2003, ApJ, 597, 142
Milosavljević M., Merritt D., 2003, ApJ, 596, 860

Miluzio M., et al., 2013, A&A, 554, A127
Minkowski R., 1941, PASP, 53, 224
Modjaz M., Gutiérrez C. P., Arcavi I., 2019, Nature Astronomy, 3, 717
Morozova V., Piro A. L., Valenti S., 2017, ApJ, 838, 28
Morris T., Podsiadlowski P., 2007, Science, 315, 1103
Nadezhin D. K., 1980, Ap&SS, 69, 115
Nadezhin D. K., 1985, Ap&SS, 112, 225
Nenkova M., Sirocky M. M., Ivezić Ž., Elitzur M., 2008a, ApJ, 685, 147
Nenkova M., Sirocky M. M., Nikutta R., Ivezić Ž., Elitzur M., 2008b, ApJ, 685, 160
Netzer H., 2013, The Physics and Evolution of Active Galactic Nuclei
Netzer H., Elitzur M., Ferland G. J., 1985, ApJ, 299, 752
Neustadt J. M. M., Kochanek C. S., Stanek K. Z., Basinger C. M., Jayasinghe T., Garling C. T., Adams S. M., Gerke J., 2021, arXiv e-prints, p. arXiv:2104.03318
Nicholl M., et al., 2019, MNRAS, 488, 1878
Nyholm A., et al., 2020, A&A, 637, A73
O'Connor E., Ott C. D., 2011, ApJ, 730, 70
Ohyama N., 1963, Progress of Theoretical Physics, 30, 170
Osterbrock D. E., Pogge R. W., 1985, ApJ, 297, 166
Owocki S. P., Rybicki G. B., 1984, ApJ, 284, 337
Padovani P., et al., 2017, A&Ar, 25, 2
Pastorello A., et al., 2007, Nature, 447, 829
Patat F., Barbon R., Cappellaro E., Turatto M., 1994, A&A, 282, 731
Patat F., et al., 2001, ApJ, 555, 900
Penston M. V., Perez E., 1984, MNRAS, 211, 33P
Pérez-Torres M. A., Romero-Cañizales C., Alberdi A., Polatidis A., 2009, A&A, 507, L17
Pérez-Torres M., Mattila S., Alonso-Herrero A., Aalto S., Efstathiou A., 2021, A&Ar, 29, 2
Peterson B. M., et al., 2004, ApJ, 613, 682
Pfister H., Bar-Or B., Volonteri M., Dubois Y., Capelo P. R., 2019, MNRAS, 488, L29
Phinney E. S., 1989, in Morris M., ed., Vol. 136, The Center of the Galaxy. p. 543
Piran T., Svirski G., Krolik J., Cheng R. M., Shiokawa H., 2015, ApJ, 806, 164
Piro A. L., 2013, ApJl, 768, L14
Podsiadlowski P., 1992, PASP, 104, 717
Podsiadlowski P., Joss P. C., Hsu J. J. L., 1992, ApJ, 391, 246
Ptak A., et al., 2015, ApJ, 800, 104
Rakshit S., Stalin C. S., Chand H., Zhang X.-G., 2017, ApJs, 229, 39
Ramos Almeida C., Ricci C., 2017, Nature Astronomy, 1, 679
Rees M. J., 1988, Nature, 333, 523
Remillard R. A., McClintock J. E., 2006, ARA&A, 44, 49
Reynolds T. M., Fraser M., Gilmore G., 2015, MNRAS, 453, 2885
Reynolds T. M., et al., 2020, MNRAS, 493, 1761
Reynolds T. M., Mattila S., Kankare E., Efstathiou A., Kool E., Ryder S., Pérez-Torres M. A., 2021, To be submitted to A&A
Rodríguez Zaurín J., Tadhunter C. N., Rose M., Holt J., 2013, MNRAS, 432, 138
Rossi E. M., Stone N. C., Law-Smith J. A. P., Macleod M., Lodato G., Dai J. L., Mandel I., 2021, Space Sci. Rev., 217, 40
Rubin A., et al., 2016, ApJ, 820, 33
Ruiz M., Shapiro S. L., Tsokaros A., 2018, Phys. Rev. D, 97, 021501
Salasnich B., Bressan A., Chiosi C., 1999, A&A, 342, 131
Salpeter E. E., 1955, ApJ, 121, 161
Sana H., James G., Gosset E., 2011, MNRAS, 416, 817
Sana H., et al., 2012, Science, 337, 444
Sanders D. B., Phinney E. S., Neugebauer G., Soifer B. T., Matthews K., 1989, ApJ, 347, 29

Sanders D. B., Mazzarella J. M., Kim D. C., Surace J. A., Soifer B. T., 2003, AJ, 126, 1607
Sanders N. E., et al., 2015, ApJ, 799, 208
Saxton R., Komossa S., Auchettl K., Jonker P. G., 2020, Space Sci. Rev., 216, 85
Schawinski K., et al., 2008, Science, 321, 223
Schlegel E. M., 1990, MNRAS, 244, 269
Schrøder S. L., Batta A., Ramirez-Ruiz E., 2018, ApJl, 862, L3
Shakura N. I., Sunyaev R. A., 1976, MNRAS, 175, 613
Shaviv N. J., 2000, ApJl, 532, L137
Shibata M., Zhou E., Kiuchi K., Fujibayashi S., 2019, Phys. Rev. D, 100, 023015
Smartt S. J., 2015, , 32, e016
Smartt S. J., Eldridge J. J., Crockett R. M., Maund J. R., 2009, MNRAS, 395, 1409
Smith N., 2007, AJ, 133, 1034
Smith N., 2017, Interacting Supernovae: Types IIn and Ibn. p. 403, doi:10.1007/978-3-319-21846-5˙38
Smith N., Frew D. J., 2011, MNRAS, 415, 2009
Smith N., Owocki S. P., 2006, ApJl, 645, L45
Smith N., Tombleson R., 2015, MNRAS, 447, 598
Smith N., Humphreys R. M., Davidson K., Gehrz R. D., Schuster M. T., Krautter J., 2001, AJ, 121, 1111
Smith J. E., Young S., Robinson A., Corbett E. A., Giannuzzo M. E., Axon D. J., Hough J. H., 2002, MNRAS, 335, 773
Smith N., Gehrz R. D., Hinz P. M., Hoffmann W. F., Hora J. L., Mamajek E. E., Meyer M. R., 2003, AJ, 125, 1458
Smith N., Li W., Silverman J. M., Ganeshalingam M., Filippenko A. V., 2011a, MNRAS, 415, 773
Smith N., et al., 2011b, ApJ, 732, 63
Smith N., et al., 2015, MNRAS, 449, 1876
Soifer B. T., et al., 2001, AJ, 122, 1213
Stone N., Sari R., Loeb A., 2013, MNRAS, 435, 1809
Stone N. C., Vasiliev E., Kesden M., Rossi E. M., Perets H. B., Amaro-Seoane P., 2020, Space Sci. Rev., 216, 35
Strolger L.-G., et al., 2015, ApJ, 813, 93
Sukhbold T., Ertl T., Woosley S. E., Brown J. M., Janka H. T., 2016, ApJ, 821, 38
Svirski G., Nakar E., 2014, ApJl, 788, L14
Tadhunter C., Spence R., Rose M., Mullaney J., Crowther P., 2017, Nature Astronomy, 1, 0061
Tadhunter C., Patel M., Mullaney J., 2021, MNRAS, 504, 4377
Tartaglia L., et al., 2020, A&A, 635, A39
Tartaglia L., et al., 2021, ApJ, 907, 52
Terreran G., et al., 2016, MNRAS, 462, 137
Trakhtenbrot B., et al., 2019, Nature Astronomy, 3, 242
Tran H. D., Osterbrock D. E., Martel A., 1992, AJ, 104, 2072
Ulrich M.-H., Maraschi L., Urry C. M., 1997, ARA&A, 35, 445
Ulvestad J. S., 2009, AJ, 138, 1529
Väisänen P., Reunanen J., Kotilainen J., Mattila S., Johansson P. H., Ramphul R., Romero-Cañizales C., Kuncarayakti H., 2017, MNRAS, 471, 2059
Valenti S., et al., 2015, MNRAS, 448, 2608
Valtonen M. J., et al., 2008, Nature, 452, 851
Van Dyk S. D., et al., 2018, ApJ, 860, 90
Vanbeveren D., Mennekens N., Van Rensbergen W., De Loore C., 2013, A&A, 552, A105
Vanden Berk D. E., et al., 2004, ApJ, 601, 692
Veilleux S., et al., 2009, ApJs, 182, 628
Vink J. S., de Koter A., Lamers H. J. G. L. M., 2001, A&A, 369, 574
Wang J., Merritt D., 2004, ApJ, 600, 149
Waxman E., Katz B., 2017, Shock Breakout Theory. p. 967, doi:10.1007/978-3-319-21846-5_33

Weiler K. W., Sramek R. A., Panagia N., van der Hulst J. M., Salvati M., 1986, ApJ, 301, 790
Wellstein S., Langer N., 1999, A&A, 350, 148
Wheeler J. C., Levreault R., 1985, ApJl, 294, L17
Woosley S. E., 1993, ApJ, 405, 273
Woosley S. E., Heger A., 2012, ApJ, 752, 32
Woosley S. E., Blinnikov S., Heger A., 2007, Nature, 450, 390
Wright G. S., Joseph R. D., Meikle W. P. S., 1984, Nature, 309, 430
Xiang D., et al., 2019, ApJ, 871, 176
Yang Y., Zabludoff A. I., Zaritsky D., Lauer T. R., Mihos J. C., 2004, ApJ, 607, 258
Young P. J., Shields G. A., Wheeler J. C., 1977, ApJ, 212, 367
Zampieri L., Pastorello A., Turatto M., Cappellaro E., Benetti S., Altavilla G., Mazzali P., Hamuy M., 2003, MNRAS, 338, 711
Zapartas E., et al., 2019, A&A, 631, A5
Zauderer B. A., et al., 2011, Nature, 476, 425
Zier C., Biermann P. L., 2002, A&A, 396, 91
de Jager C., Nieuwenhuijzen H., van der Hucht K. A., 1988, A&As, 72, 259
de Mink S. E., Langer N., Izzard R. G., Sana H., de Koter A., 2013, ApJ, 764, 166
van Velzen S., 2018, ApJ, 852, 72
van Velzen S., Farrar G. R., 2014, ApJ, 792, 53
van Velzen S., et al., 2011, ApJ, 741, 73
van Velzen S., et al., 2016a, Science, 351, 62
van Velzen S., Mendez A. J., Krolik J. H., Gorjian V., 2016b, ApJ, 829, 19
van Velzen S., Holoien T. W. S., Onori F., Hung T., Arcavi I., 2020, Space Sci. Rev., 216, 124
van Velzen S., et al., 2021, ApJ, 908, 4

TURUN
YLIOPISTO
UNIVERSITY
OF TURKU

Painosalama, Turku, Finland 2021

ISBN 978-951-29-8650-7 (PRINT)
ISBN 978-951-29-8651-4 (PDF)
ISSN 0082-7002 (PRINT)
ISSN 2343-3175 (ONLINE))